Computer Modeling in Engineering & Sciences

Tech Science Press

Doi:10.32604/cmes.2025.072973

ARTICLE

Robust Control and Stabilization of Autonomous Vehicular Systems under Deception Attacks and Switching Signed Networks

Muflih Alhazmi[1], Waqar Ul Hassan[2], Saba Shaheen[3], Mohammed M. A. Almazah[4], Azmat Ullah Khan Niazi[3,*], Nafisa A. Albasheir[5], Ameni Gargouri[6] and Naveed Iqbal[7]

[1]Department of Mathematics, College of Sciences, Northern Border University, Arar, 91413, Saudi Arabia
[2]Department of Mathematics, Faculty of Sciences, University of Mianwali, Mianwali, 42200, Punjab, Pakistan
[3]Department of Mathematics and Statistics, The University of Lahore, Sargodha, 40100, Pakistan
[4]Department of Mathematics, College of Sciences and Arts (Muhyil), King Khalid University, Muhyil, 61421, Saudi Arabia
[5]Department of Mathematics, College of Sciences and Arts (Magardah), King Khalid University, Magardah, 61421, Saudi Arabia
[6]Mathematics Department, College of Humanities and Science in Al Aflaj, Prince Sattam Bin Abdulaziz University, Al-Kharj, 11912, Saudi Arabia
[7]Department of Mathematics, College of Science, University of Ha'il, Ha'il, 2440, Saudi Arabia

*Corresponding Author: Azmat Ullah Khan Niazi. Email: azmatullah.khan@math.uol.edu.pk

Received: 08 September 2025; Accepted: 27 October 2025; Published: 26 November 2025

ABSTRACT: This paper proposes a model-based control framework for vehicle platooning systems with second-order nonlinear dynamics operating over switching signed networks, time-varying delays, and deception attacks. The study includes two configurations: a leaderless structure using Finite-Time Non-Singular Terminal Bipartite Consensus (FNTBC) and Fixed-Time Bipartite Consensus (FXTBC), and a leader—follower structure ensuring structural balance and robustness against deceptive signals. In the leaderless model, a bipartite controller based on impulsive control theory, gauge transformation, and Markovian switching Lyapunov functions ensures mean-square stability and coordination under deception attacks and communication delays. The FNTBC achieves finite-time convergence depending on initial conditions, while the FXTBC guarantees fixed-time convergence independent of them, providing adaptability to different operating states. In the leader—follower case, a discontinuous impulsive control law synchronizes all followers with the leader despite deceptive attacks and switching topologies, maintaining robust coordination through nonlinear corrective mechanisms. To validate the approach, simulations are conducted on systems of five and seventeen vehicles in both leaderless and leader—follower configurations. The results demonstrate that the proposed framework achieves rapid consensus, strong robustness, and high resistance to deception attacks, offering a secure and scalable model-based control solution for modern vehicular communication networks.

KEYWORDS: Autonomous vehicles; vehicle platooning; stabilization; decision and control systems; switching signed networks; leader–follower coordination; gauge transformation; Lyapunov stability; deception and cybe-security attacks; secure vehicular networks

1 Introduction

Vehicular networking has become essential in modern intelligent transportation systems, enabling efficient communication for safety and coordination among vehicles. With 5G technology offering ultra-reliable and low-latency links, such networks support advanced applications requiring real-time responsiveness [1]. Recent research in vehicular ad hoc networks (VANETs) has emphasized enhancing routing stability,

communication reliability, and control robustness through predictive and trajectory-based approaches. Predictive modeling techniques forecast future vehicular states, enabling routing algorithms to sustain reliable communication links even under rapidly changing mobility conditions [2]. Similarly, bus-trajectory-based street-centric routing leverages predefined bus routes to optimize message delivery and reduce latency in dense urban environments [3]. Furthermore, recent advances in prescribed-time optimal control for switched nonlinear systems provide a powerful framework for achieving optimal-precision coordination within vehicular platoons, ensuring that stability and convergence are attained within a user-defined time despite switching network and system nonlinearities [4]. Decision-making and motion planning frameworks ensure smooth, oscillation-free movement by coordinating perception and control modules [5]. Focuses on the importance of protecting vehicle location privacy to ensure secure communication and prevent tracking in intelligent transportation systems. Emphasizes privacy preservation as a key factor for safety and trust in vehicular networks [6]. Furthermore, semi-global stabilization of parabolic systems with input saturation ensures stability under actuator constraints using Lyapunov and back-stepping-based control, enhancing robustness in distributed vehicular dynamics [7]. Recent advancements in intelligent transportation and autonomous control systems focus on adaptive and resilient designs to ensure stability, coordination, and safety in dynamic environments. Knowledge-guided self-learning control strategies enhance mixed vehicle platoon performance under communication delays, while cognitive risk prediction models utilize spatiotemporal features to assess human driving behavior and prevent potential hazards [8,9]. Coordinated tracking control of integrated wheel-end systems supports precise motion management, and advanced identification algorithms improve network stability and fault detection in complex control structures for the surveillance task schedule [10,11]. Enhanced localization techniques using Low Earth Orbit (LEO) satellite signals strengthen real-time positioning accuracy in uncertain conditions [12]. Furthermore, recurrent neural network–based sliding mode control provides robust stabilization for uncertain tilting quad rotor UAVs by handling external disturbances and modeling errors, while AI-driven perturbation defense techniques ensure accurate recognition of ultra high-speed weak targets, thereby reinforcing the reliability and intelligence of autonomous aerial and vehicular systems [13,14]. The intelligent vehicular systems highlights the integration of advanced testing, sensing, modeling, and resilient control strategies to ensure safety, autonomy, and robustness in dynamic environments. Adversarial scenario generation using hierarchical reinforcement architectures provides rigorous validation for intelligent vehicles, while high-fidelity ultrasonic radar in-the-loop testing enables realistic assessment of automatic parking systems [15,16]. Lane-changing models that incorporate human driving behavior and spatiotemporal decision features enhance motion prediction and cooperative driving accuracy [17,18].

Adaptive PI event-triggered control strategies for nonlinear systems with input delays enhance system responsiveness and robustness against time-varying uncertainties, contributing to improved stability in networked control environments [19]. The trade-off between code estimation error rate and terminal gain has been analyzed to strengthen communication reliability and resilience against adversarial disturbances in vehicle networks [20]. Furthermore, an improved social force model based on pedestrian collision avoidance behavior in counterflow conditions provides deeper insight into dynamic interactions within mixed traffic environments, improving safety and flow efficiency [21]. A hybrid framework combining neural networks with physics-based estimators enables accurate vehicle longitudinal dynamics modeling using limited driving data, bridging the gap between data-driven learning and physical interpretability [22]. Distributed safety-critical formation control using contracting bearing estimators and control barrier functions ensures reliable coordination among connected vehicles under sensing and communication limitations [23]. Finally, intelligent event-triggered lane-keeping security control mechanisms for autonomous vehicles under Denial-of-Service (DoS) attacks significantly enhance communication efficiency and cyber-resilience in connected

vehicular networks [24]. Finally, stability and stabilization principles for sampled-data Lurie systems provide theoretical foundations supporting the implementation of these intelligent control strategies in discrete-time vehicular applications [25].

The intelligent autonomous systems and robust control highlights advances in perception, learning, and cooperative navigation to ensure safe and efficient decision-making in complex environments. Human interaction recognition using extended filtering improves behavior estimation and interaction awareness, while real-time contactless eye-blink detection enhances driver safety by monitoring fatigue without physical sensors [26,27]. Interaction-aware trajectory prediction based on transformer-driven transfer learning enables proactive motion planning by forecasting surrounding agents' intentions, thus improving collision avoidance and cooperative driving efficiency [28,29]. Robust localization frameworks integrating multi-sensor fusion and synchronization algorithms ensure precise navigation performance despite urban signal interference and noise [30,31]. Additionally, noise-tolerant and predefined-time zeroing neural networks offer resilient synchronization and rapid dynamic computations for nonlinear systems, supporting stable control performance under disturbances [32,33]. Furthermore, vehicle-assisted service caching and task offloading in vehicular edge computing, when combined with Nash-equilibrium-based robust control under servo constraints, significantly enhance distributed coordination, reduce latency, and enable adaptive cooperative operation in autonomous and humanoid robotic systems [34,35].

Research on vehicular perception and control emphasizes adaptive learning and deception-resilient recognition to ensure reliability and safety in dynamic driving environments. A neural network incorporating plasticity effectively detects driver fatigue on real roads by adapting to changing behavioral and physiological patterns while resisting deceptive signal variations that may mask true driver conditions [36]. Likewise, a self-supervised evaluation method using a hyper graph neural network with dynamic feature learning accurately assesses insulation conditions in vehicle cable terminals, remaining robust against deceptive or corrupted sensor inputs that could threaten electrical stability and safety [37]. Together, these studies highlight how adaptive and self-learning neural models strengthen resilience and situational awareness in modern vehicular systems. Research on cyber–physical resilience and deception-resistant control in vehicular and transportation networks integrates detection, coordination, and adaptive learning to counter malicious interference and data manipulation. A DDoS detection framework using interquartile range and deep feature fusion convolutional networks identifies abnormal traffic behaviors in software-defined systems, serving as the first layer of defense against large-scale deception-based disruptions [38]. Complementing this, AST-based static fuzz mutation enhances software reliability by identifying concurrency vulnerabilities that attackers might exploit to inject deceptive commands or data anomalies [39]. Presents distributed robust finite-time consensus protocols designed for nonlinear multi-agent systems under uncertainties and disturbances. Emphasizes rapid convergence and resilience, ensuring system stability within a finite time through decentralized control strategies [40]. Perception task-oriented information sharing across autonomous vehicles further strengthens system awareness, enabling robust response to occlusion-based or deceptive sensory manipulation [41]. To ensure secure dynamic control, fixed-time safe tracking for uncertain nonlinear systems achieves rapid recovery and resilience against feedback distortion or deceptive control signals [42]. Finally, machine learning-driven analysis of transport infrastructure connectivity and conflict resolution enhances system resilience by detecting hidden anomalies and strategic deception within large-scale transportation data [43]. Moreover, recent robust adaptive control strategies further strengthen platoon coordination by incorporating disturbance estimation, compensation, and resilience against network disconnections and finite-time networks [44,45], ensuring reliable and secure operation across varying traffic and communication conditions in complex fractional-order networks.

Motivated by the challenges of maintaining coordination and stability in nonlinear vehicle platoons affected by time-varying delays, switching topologies, and deception attacks, this study presents a unified model-based control framework integrating both finite-time and fixed-time bipartite consensus schemes. The main contributions are as follows:

- A distributed impulsive control protocol is designed to achieve Finite-Time Non-Singular Terminal Bipartite Consensus (FNTBC) and Fixed-Time Bipartite Consensus (FXTBC) under switching signed networks, ensuring rapid convergence and resilience to communication disturbances.
- A deception-attack detection and suppression mechanism is incorporated within impulsive control events, enhancing network security and maintaining synchronization accuracy under malicious data manipulation.
- The vehicle dynamics are modeled as second-order nonlinear systems capturing both position and velocity behaviors, accurately reflecting realistic platoon interactions.
- A delay-compensated control strategy is introduced to handle time-varying communication delays, preserving coordinated motion despite asynchronous updates.
- The stability and boundedness of the proposed framework are rigorously established using Lyapunov theory, impulsive differential systems, and Markovian switching models.
- The overall framework operates using only local information, making it scalable and implementable in large-scale vehicular communication networks.

The following sections make up the rest of this paper:

1. Section 1 provides background information and research motivation, and the primary contributions of the study.
2. Section 2 provides a brief overview of graph theory basics before moving on to analyze impulsive systems under finite- and fixed-time stability conditions with their required assumptions and definitions, and problem formulation.
3. Section 3 contains the main analytical results, which include leaderless and leader-following control strategies for finite-time and fixed-time bounded consensus in networked vehicle systems, supported by four principal theorems.
4. Section 4 presents simulation results which confirm the effectiveness of the proposed control methods.
5. Section 5 of the paper presents essential findings together with recommendations for additional research.

2 Problem Statement

2.1 Graph Theory

A signed graph $G = (V, E, \mathcal{A})$ represents a vehicle platooning. The set of nodes is given as $V = \{1, 2, 3, \ldots, M\}$ representing individual vehicles in this model. The set of edges $E \subseteq V \times V$ represents the communication links that connect pairs of vehicles. The communication network structure is encoded in the weighted adjacency matrix $\mathcal{A} = [a_{mn}] \in \mathbb{R}^{M\times M}$, which describes the interactions between these vehicles.

A nonzero weight $a_{mn} \neq 0$ value shows that there exists an edge connecting nodes m and n such that $(m, n) \in E$. The neighborhood of vehicle m is defined as $N_m = \{n \mid a_{mn} \neq 0\}$. The signed graph G is undirected if the edge set meets the condition $(m, n) \in E \Leftrightarrow (n, m) \in E$.

The weights a_{mn} may be either positive or negative; a positive weight $a_{mn} > 0$ means that the vehicles are cooperative with each other, while a negative weight $a_{mn} < 0$ means that the vehicles are adversarial with each other. A sequence of edges such as $(m_1, m_2), (m_2, m_\ell), \ldots, (m_{k-1}, m_k)$. Where all intermediate nodes m_ℓ for $\ell = 1, 2, \ldots, k$ are distinct, is referred to as a path from node m_1 to node m_k.

A graph is considered connected if, for any pair of distinct nodes m and n where $m \neq n$, there exists a path connecting them. The Laplacian matrix $\mathcal{L} = [\ell_{mn}] \in \mathbb{R}^{M\times M}$ for a signed graph G is defined such that the diagonal elements are given as $\ell_{mm} = \sum_{\substack{n=1 \\ n\neq m}}^{M} |a_{mn}|$.

The off-diagonal entries are $\ell_{mn} = -a_{mn}$, for $m \neq n$. The network becomes an augmented graph $\hat{G} = (\hat{V}, \hat{E})$ by adding a leader node, indexed as node 0. The node set transforms into $\hat{V} = V \cup \{0\}$ while the edge set becomes $\hat{E} \subseteq \hat{V} \times \hat{V}$. A communication link from the leader to the vehicle $m \in V$ is established if $a_{m0} > 0$, the leader shares information with the vehicle otherwise $a_{m0} = 0$. The diagonal matrix $\mathcal{S}_0 = \text{diag}(a_{10}, a_{20}, \ldots, a_{M0})$ represents the leader's influence power within the network structure. The modified Laplacian matrix takes into account the leader's input through this expression $\mathcal{L}_0 = \mathcal{L} + \mathcal{S}_0$.

Lemma 1. *[46] A signed graph G is structurally balanced if it contains a spanning tree. The Laplacian matrix $\mathcal{L}_0$, which includes the leader's influence, becomes positive definite when the leader node acts as the root of this spanning tree in a structurally balanced network signed graph $\hat{G}$. This ensures both structural coherence and stability in the network.*

Definition 1. *[46] A signed graph G is considered structurally balanced if its node set V can be divided into two disjoint subsets V_1 and V_2 such that*

$$V_1 \cap V_2 = \varnothing, \quad V_1 \cup V_2 = V.$$

The edge weights satisfy the condition $a_{mn} \geq 0$ when both nodes m and n are in the same subset V_q while $a_{mn} \leq 0$ when $m \in V_q$ and $n \in V_{3-q}$, in which $q \in \{1, 2\}$. If such a partition does not exist, the graph is termed structurally unbalanced. To formalize this concept, the set $\mathcal{D}$ defined as

$$\mathcal{D} = \{D = \text{diag}(d_1, d_2, d_3, \ldots, d_M) \,|\, d_m \in \{1, -1\}\}.$$

Each matrix $D \in \mathcal{D}$ corresponds to a particular partitioning of the graph, where nodes are assigned according to the sign of d_m.

$$V_1 = \{m \mid d_m = 1\}, \quad V_2 = \{m \mid d_m = -1\} \quad for \quad m \in V$$

The following vehicle platooning provides conditions that are equivalent to the structural balance of the graph.

Lemma 2. *[46] A signed graph G is said to be connected and structurally balanced if it satisfies the following conditions*

- *A diagonal matrix $D \in \mathcal{D}$ exists which transforms the matrix $D\mathcal{A}D$ into a form where all entries are nonnegative.*
- *The associated Laplacian matrix $\mathcal{L}$ is positive semidefinite, having exactly one eigenvalue equal to zero.*

Lemma 3. *The bipartite consensus formulation uses the gauge transformation $D = \text{diag}(d_1, d_2, \ldots, d_M)$ with $d_i \in \{1, -1\}$. The transformation $D^T D = I$ results in an orthogonal matrix that maintains the original norm values of the input vectors $\|Dx\| = \|x\|$, $\|Dv\| = \|v\|$.*

The mapping $x \mapsto Dx$, $v \mapsto Dv$ leaves all vehicle state constraints of the form $|x_i(t)| \leq x_{\max}$ and $|v_i(t)| \leq v_{\max}$ unchanged. The transformed Laplacian $\mathcal{L}' = D\mathcal{L}D$ retains the spectral characteristics of $\mathcal{L}$ and maintains a bounded Lyapunov function $V(t) = \frac{1}{2}H^T H$. The gauge transformation maintains constraint satisfaction because it prevents the transformed consensus dynamics from increasing system state values.

Remark 1. *Lemma 3 demonstrates that the gauge transformation maintains bounded vehicle states because it protects the absolute values of the states. The transformation between cooperative and competitive clusters*

only changes the sign of the states but keeps their magnitudes unchanged, which results in physically valid state trajectories for bipartite consensus.

Remark 2. *In this work, we assume that external disturbances (such as aerodynamic drag, tire friction variation, road slope, and wind) are bounded or sufficiently small relative to the primary destabilizing effects considered. According to recent studies such as [47], network disconnections and communication delays rank among the top contributors to platoon instability, whereas external disturbances, while non-negligible, have a smaller relative impact. Under this assumption, we focus primarily on mitigating communication-based uncertainties and deception attacks.*

2.2 Analysis of Impulsive Systems under Finite-Time and Fixed-Time Stability

Vehicle platooning consists of M vehicles that demonstrate nonlinear impulsive behavior. The dynamics of each vehicle are characterized by the following equations

$$\begin{cases} \dot{x}_m(t) = v_m(t), & x_m(t_0) = x_{m0}, & \text{for } t \neq t_p, \\ \dot{v}_m(t) = z_e(v_m(t)), & v_m(t_0) = v_{m0}, & \text{for } t \neq t_p, \\ \Upsilon x_m(t) = z_d(x_m(t)), & & \text{at } t = t_p, \\ \Upsilon v_m(t) = z_d(v_m(t)), & & \text{at } t = t_p. \end{cases} \tag{1}$$

The state vector of the mth vehicle is represented by $x_m(t) \in \mathbb{R}^l$ and $v_m(t) \in \mathbb{R}^l$ composed of its position and velocity in Eq. (1). The system evolves continuously through $z_e : \mathbb{R}^l \times \mathbb{R}^+ \to \mathbb{R}^l$, which governs the vehicle's dynamics between the impulsive moments and is assumed to be a continuous mapping. The discrete (impulsive) behavior is described by the function $z_d : \mathbb{R}^l \times \mathbb{R}^+ \to \mathbb{R}^l$, which is also a continuous function. Each impulsive event at time t_p results in a state change of the vehicle according to

$$\Upsilon x_m(t_p) = x_m(t_p^+) - x_m(t_p)$$
$$\Upsilon v_m(t_p) = v_m(t_p^+) - v_m(t_p).$$

The state vector $x_m(t)$, $v_m(t)$ remains left-continuous which means $x_m(t_p^-) = x_m(t_p)$, $v_m(t_p^-) = v_m(t_p)$ while the post-impulse state can be equivalently expressed as $x_m(t_p^+) = x_m(t_p^-) + \Upsilon x_m(t)$, $v_m(t_p^+) = v_m(t_p^-) + \Upsilon v_m(t)$. This framework provides a rigorous basis for the analysis of how impulsive effects contribute to the finite-time or fixed-time stabilization of the overall system.

Lemma 4. *[48] Suppose $\psi_1, \psi_2, \ldots, \psi_\ell \geq 0$ with parameters $0 < k \leq 1$ and $l > 1$. The following inequalities are satisfied*

$$\sum_{m=1}^{\ell} \psi_m^k \geq \left(\sum_{m=1}^{\ell} \psi_k \right)^k, \quad \sum_{m=1}^{\ell} \psi_m^l \geq \ell^{1-l} \left(\sum_{m=1}^{\ell} \psi_m \right)^l \tag{2}$$

These results show that under the given conditions, the kth and lth powers of non-negative sequences are bounded by the sum of the original elements.

Lemma 5. *[49] Let's analyze the nonlinear impulsive system defined by Eq. (1) and suppose there be a function $\mathcal{V}(x_m, v_m)$ such that for all times $t \neq t_p$ the inequality $\dot{\mathcal{V}}(x_m, v_m)\, z_e(x_m, v_m) \leq -e\, (\mathcal{V}(x_m, v_m))^w$ holds, and at the impulse times $t = t_p$ it must fulfills $\mathcal{V}(x_m, v_m(t_p^+)) \leq \mathcal{V}(x_m, v_m(t_p^-))$. In this context, where $e > 0$ and $0 < w < 1$ the impulsive system is guaranteed to be finite-time stable. Moreover, the finite settling time $\mathcal{T}$, taken*

by the state to reach the origin, is given as

$$\mathcal{T} \leq \frac{\mathcal{V}(x_m(0), v_m(0))^{1-w}}{e(1-w)}$$

Lemma 6. *[50] Consider a system characterized by a bounded impulsive interval $\chi^p = t_{p+1} - t_p$ defined over an impulsive sequence $\epsilon = \{t_p\}(p \in \mathbb{N})$ with χ_1 and χ_2 as the maximum and minimum bounds of χ^p. Assume that there is a scalar function $\mathcal{V}(x_m, v_m)$ that satisfies the following conditions*

1. For all $t \neq t_p$ the function is bounded as $u_1 \|x_m(t), v_m(t)\|_\xi \leq \mathcal{V}(x_m(t), v_m(t)) \leq u_2 \|x_m(t), v_m(t)\|_\xi$

2. The jump condition $\mathcal{V}(x_m(t_p^+), v_m(t_p^+)) \leq \lambda \mathcal{V}(x_m(t_p), v_m(t_p))$ applies for every impulsive instant $t = t_p$. Under these assumptions, the system Eq. (1) is guaranteed to reach a fixed-time stable state. The total convergence time $\mathcal{T}$ is given as

- *For $\lambda = 1$*

$$\mathcal{T} = \frac{1}{\psi(1-b)} + \frac{1}{\gamma(c-1)}$$

- *For $0 < \lambda < 1$*

$$\mathcal{T} = \frac{\chi_1}{(1-c)\ln\lambda} \ln\left(1 - \frac{\lambda^{1-c}\ln\lambda}{\gamma\chi_1}\right) + \frac{\chi_1}{(1-b)\ln\lambda} \ln\left(1 + \frac{\ln\lambda}{\psi\chi_2\lambda^{2(1-c)} - \ln\lambda}\right)$$

Such that all the constants fulfill

$$u_1 > 0, \quad u_2 > 0, \quad p > 0, \quad \psi > 0, \quad \gamma > 0, \quad 0 < b < 1, \quad c > 1, \quad \text{and} \quad 0 < \lambda \leq 1$$

3. The derivative of $\mathcal{V}$ when $t \neq t_p$ can be expressed as

$$\dot{\mathcal{V}}(x_m(t), v_m(t)) \leq \begin{cases} -\psi\, \mathcal{V}^b(x_m(t), v_m(t)), & 0 < \mathcal{V}(x_m(t), v_m(t)) \leq 1, \\ -\gamma\, \mathcal{V}^c(x_m(t), v_m(t)), & \mathcal{V}(x_m(t), v_m(t)) > 1, \\ 0, & \mathcal{V}(x_m(t), v_m(t)) = 0. \end{cases}$$

2.3 Problem Formulation

Examine a second-order vehicle platooning consisting of M vehicles that communicate through an undirected signed graph G. The following describes the dynamics of the leader's behavior.

$$\begin{cases} \dot{x}_0(t) = v_0(t) \\ \dot{v}_0(t) = u_0(t) \end{cases} \tag{3}$$

where $(x_0(t), v_0(t)) \in \mathbb{R}^l$ denote the position and velocity of the leader while $u_0(t) \in \mathbb{R}^l$ represents its control input vector, which determines the state evolution over time.

The dynamic behavior of each vehicle is modeled as

$$\begin{cases} \dot{x}_m(t) = v_m(t) \\ \dot{v}_m(t) = u_m(t) \quad m \in V \end{cases} \tag{4}$$

The control input is given as $u_m(t) \in \mathbb{R}^l$, while, $(x_0(t), v_0(t)) \in \mathbb{R}^l$ denote the position and velocity of the mth vehicle. The network contains a specific leader in certain cases, and other vehicles must follow or synchronize their states with this leader.

Assumption 1. *The leaderless system Eq. (3) operates under the assumption that the interaction graph remains structurally balanced and connected, which enables reliable information exchange and vehicle state alignment. The leader-following framework uses systems Eqs. (3) and (4) under the assumption that the communication topology G contains a directed spanning tree with the leader positioned at the root. The network structure ensures that the leader's information reaches all followers either directly or indirectly.*

The set of nodes in the signed graph G can be divided into two disjoint subsets V_1 and $V2$, according to assumption (1) reflecting the structurally balanced nature of the network. The main objective is to design a class of impulsive control strategies that can steer the vehicles to bipartite consensus within a finite or fixed time horizon, as formally stated in the following section.

Definition 2. *Considering a leaderless vehicle platooning governed by system (4) is said to achieve finite-time bipartite consensus if, for some appropriate control input u_m and a finite time $\mathcal{T} > 0$ which may depend on the initial conditions of vehicles, for any (x_0, v_0) the following condition must satisfied,*

$$\lim_{t\to\mathcal{T}}(x_m(t), v_m(t)) = d_m\rho, \quad m \in V \tag{5}$$

where ρ is a constant and $d_m \in \{\pm 1\}$. This means that the state $(x_m(t), v_m(t))$ converges to either ρ or $-\rho$ within time $\mathcal{T}$, based on the value of d_m. Here, $\mathcal{T}$ is called the settling time. The leader-following vehicle platooning described by systems (3) and (4) requires the following condition for finite time bipartite consensus (FNTBC).

$$\lim_{t\to\mathcal{T}} \|(x_m(t), v_m(t)) - d_m(x_0(t), v_0(t))\| = 0, \quad m \in V \tag{6}$$

If the $d_m = 1$ then the mth vehicle belongs to V_1; otherwise, $d_m = -1$. Furthermore, a system reaches fixed-time bipartite consensus when the settling time $\mathcal{T}$ remains independent of initial states.

3 Main Results

This section examines control mechanisms for both leaderless and leader-driven vehicle platooning under finite-time and fixed-time boundary consensus protocols. The mechanisms operate within an impulsive control framework to achieve coordination under specified convergence criteria.

3.1 Leaderless Finite-Time Bipartite Consensus (FNTBC) and Fixed-Time Bipartite Consensus (FXTBC) in Networked Vehicles

The concepts of Finite-Time Non-Singular Terminal Bipartite Consensus (FNTBC) and Fixed-Time Bipartite Consensus (FXTBC) play crucial roles in ensuring rapid coordination among networked vehicles. Although both aim to achieve bipartite consensus in a finite duration, their convergence characteristics differ significantly.

Specifically, FNTBC guarantees that the consensus among agents is reached within a finite time that depends on the initial conditions of the system. The convergence rate in this case varies with the magnitude of initial errors, leading to fast stabilization when initial discrepancies are small. In contrast, FXTBC achieves convergence within a fixed upper bound of time, completely independent of the initial conditions. This is realized by introducing additional nonlinear corrective terms with exponents greater than one, which strengthen the control action as the system approaches equilibrium.

From a practical perspective, FNTBC is efficient when the initial state differences among vehicles are moderate and known, while FXTBC is more suitable for scenarios where initial states are highly uncertain, such as large-scale vehicle platoons or dynamically changing environments.

3.1.1 Leaderless Finite-Time Bipartite Consensus (FNTBC)

The finite time bipartite consensus (FNTBC) criterion from Eq. (5) for the vehicle platooning dynamics modeled in Eq. (4) requires a strategically designed impulsive control scheme that uses discontinuous impulses and nonlinear consensus dynamics to achieve finite-time boundary convergence. The impulsive control protocol is extended to handle both communication delays and malicious deception attacks for more realistic vehicle platooning dynamics. The control input for the mth vehicle is modified,

$$u_m(t-\tau) = \begin{cases} e_0 \sum_{n=1}^{M} a_{mn}\ \mathrm{sign}^{\theta}\left(x_n - \mathrm{sign}(a_{mn})x_m\right) + r_0 \sum_{n=1}^{M} a_{mn}\ \mathrm{sign}^{\theta}\left(v_n - \mathrm{sign}(a_{mn})v_m\right) \\ -\left[\sum_{p=1}^{+\infty} \alpha(t-t_p)Q(t) \sum_{n=1}^{M} |a_{mn}|\left(x_m - \mathrm{sign}(a_{mn})x_n\right)\right. \\ \left. + \sum_{p=1}^{+\infty} \beta(t-t_p)R(t) \sum_{n=1}^{M} |a_{mn}|\left(v_m - \mathrm{sign}(a_{mn})v_n\right)\right] \\ + \Gamma(t_p)\Phi\left(x_i(t_p)\right) + \Xi(t_p)\phi\left(v_i(t_p)\right) \end{cases} \tag{7}$$

where,

- x_n, v_n denote the position and velocity of agent n, respectively.
- a_{mn} is the (m,n)-th entry of the adjacency matrix representing the communication graph.
- $\mathrm{sign}^{\theta}(z)$ denotes the continuous sign function with fractional exponent $\theta \in (0,1)$, defined as $\mathrm{sign}^{\theta}(z) = |z|^{\theta} \cdot \mathrm{sign}(z)$.
- $e_0 \geq 0$ and $r_0 \geq 0$ are protocol gains for the position and velocity components.
- $Q(t)$ and $R(t)$ are time-varying impulsive gain functions applied at discrete times.
- $\alpha(t)$ and $\beta(t)$ are Dirac delta functions with the property:

$$\alpha(t) = \beta(t) = \begin{cases} +\infty, & t = 0 \\ 0, & t \neq 0 \end{cases}, \quad \int_{-\infty}^{+\infty} \alpha(t)\,dt = \int_{-\infty}^{+\infty} \beta(t)\,dt = 1,$$

  t_p denotes the impulsive update times.
- $\Gamma(t_p)\Phi(x_i(t_p)) + \Xi(t_p)\phi(v_i(t_p))$ represents a deception attack acting on the position and velocity of agent i at time t_p. The terms $\Gamma(t_p)$ and $\Xi(t_p)$ model the attack intensities, while $\Phi(\cdot)$ and $\phi(\cdot)$ describe the injected malicious signal components.

The uniformly spaced time sequence $\{t_p\}_0^{\infty}$ represents the potential occurrence of deception attacks. The system operates under $0 = t_0 < t_1 < \cdots < t_p < \cdots$ conditions, and the time intervals between impulses follow $t_p - t_{p-1} = q$, rules with $q > 0$ being a predetermined constant.

The sequences $\Gamma(t_p), \Xi(t_p)$ follows a Bernoulli distribution because the probability of $\Gamma(t_p), \Xi(t_p)$ taking the value 1 equals $\mathrm{prob}\{\Gamma(t_p), \Xi(t_p) = 1\} = \vartheta$, which leads to $\mathrm{prob}\{\Gamma(t_p), \Xi(t_p) = 0\} = 1 - \vartheta$. The function $\Phi(x_i(t_p)), \phi(v_i(t_p)) \in \mathbb{R}^{l_{x,v}}$ represents the deception attack input.

The impulsive structure enables vehicles to interact minimally yet efficiently. The proposed control protocol (7) modifies both continuous and instantaneous behavior of each vehicle to achieve finite-time convergence even with sporadic corrections.

The dynamic model for vehicle m under this scheme evolves as,

$$\begin{aligned}(\dot{x}_m(t),\dot{v}_m(t)) = {} & e_0\sum_{n=1}^{M} a_{mn}\ \mathrm{sign}^{\theta}\left(x_n-\mathrm{sign}(a_{mn})x_m\right)+r_0\sum_{n=1}^{M} a_{mn}\ \mathrm{sign}^{\theta}\left(v_n-\mathrm{sign}(a_{mn})v_m\right)\\ & -\sum_{p=1}^{+\infty}\alpha(t-t_p)Q(t)\sum_{n=1}^{M}|a_{mn}|\left(x_m-\mathrm{sign}(a_{mn})x_n\right)\\ & -\sum_{p=1}^{+\infty}\beta(t-t_p)R(t)\sum_{n=1}^{M}|a_{mn}|\left(v_m-\mathrm{sign}(a_{mn})v_n\right)\\ & +\Gamma(t_p)\Phi\left(x_i(t_p)\right)+\Xi(t_p)\phi\left(v_i(t_p)\right)\end{aligned} \tag{8}$$

Lemma 7. *The system described by Eq. (4) with the control protocol defined in (7) operates as a vehicle platooning. The weighted average state of the system, denoted by* $(\hat{x}(t),\hat{v}(t)) = \frac{1}{M}\sum_{m=1}^{M} d_m(x_m(t),v_m(t))$, *In other words,* $(\dot{\hat{x}}(t),\dot{\hat{v}}(t)) = 0$ *remains constant over time. Implying that this aggregated state is invariant throughout the system's evolution.*

Remark 3. *The control mechanism operates conventionally at times other than impulses. The vehicles experience major state changes during impulse moments. Dirac delta function activation causes this phenomenon, which results in an immediate and powerful state adjustment. The impulsive effects play a major role in speeding up the system's convergence process.*

$$\begin{cases} H(t) = \left[\ (x_1,v_1)^{\mathcal{T}}(t),(x_2,v_2)^{\mathcal{T}}(t),\ldots,(x_M,v_M)^{\mathcal{T}}(t)\ \right]^{\mathcal{T}},\\ z_e(H(t)) = \left[\ z_{e_1}^{\mathcal{T}}(x(t),v(t)),z_{e_2}^{\mathcal{T}}(x(t),v(t)),\ldots,z_{e_M}^{\mathcal{T}}(x(t),v(t))\ \right]^{\mathcal{T}},\\ z_{e_m}(x(t),v(t)) = e_0\sum_{n=1}^{M} a_{mn}\ \mathrm{sign}^{\theta}\left(x_n-\mathrm{sign}(a_{mn})x_m\right)+r_0\sum_{n=1}^{M} a_{mn}\ \mathrm{sign}^{\theta}\left(v_n-\mathrm{sign}(a_{mn})v_m\right),\\ \sum_{n=1}^{M}|a_{mn}|(x_m-\mathrm{sign}(a_{mn})x_n)+\sum_{n=1}^{M}|a_{mn}|(v_m-\mathrm{sign}(a_{mn})v_n)=\sum_{n=1}^{M}\ell_{mn}(x_n,v_n). \end{cases}$$

The original system (4) can be compactly expressed as

$$\dot{H}(t) = \begin{cases}\mathcal{F}(H(t)), & t\neq t_p\\ H(t^-)+\Upsilon(H(t^-),t_p), & t=t_p\end{cases}$$

$$\dot{H}(t) = \begin{cases}\begin{bmatrix}0 & I_M\\ -e_0\mathcal{L}_{\theta}^{x} & -r_0\mathcal{L}_{\theta}^{v}\end{bmatrix}\otimes I_l\cdot H(t), & t\neq t_p\\ \left[I_{2M}-\mathcal{D}(t_p)\right]\otimes I_l\cdot H(t_p^-)+A(t_p), & t=t_p\end{cases} \tag{9}$$

where

$$\begin{cases} H(t) = \begin{bmatrix} x(t)^\top & v(t)^\top \end{bmatrix}^\top \in \mathbb{R}^{2Ml}, & \text{is the augmented state vector,} \\ \mathcal{L}_\theta^x \text{ and } \mathcal{L}_\theta^v & \text{are nonlinear Laplacian-like matrices for position and velocity derived using the } \operatorname{sign}^\theta \text{ rule,} \\ \mathcal{D}(t_p) = \begin{bmatrix} 0 & 0 \\ Q(t_p)\mathcal{L} & R(t_p)\mathcal{L} \end{bmatrix}, & \text{represents the impulsive feedback applied at event time } t_p, \\ A(t_p) = \begin{bmatrix} 0 \\ \Gamma(t_p)\Phi(x(t_p)) + \Xi(t_p)\phi(v(t_p)) \end{bmatrix}, & \text{captures the deception attacks introduced during impulse instants.} \end{cases}$$

Theorem 1. *Consider a system of M vehicles described by second-order dynamics as in Eq. (4) following the impulsive control strategy, to reach finite-time bipartite consensus under deception attacks, which is defined by Eq. (7). The parameters should be chosen to meet the following conditions:* $e_0 > 0$, $0 < \theta < 1$, *and* $(x_m(t), v_m(t)) \in \mathbb{R}^l$. *The impulses gain functions* $Q(t)$ *and* $R(t)$ *must satisfies*

$$Q(t) \le \frac{2\mu_{\min}(\mathcal{L})}{\mu_{\max}^2(\mathcal{L})} \quad R(t) \le \frac{2\nu_{\min}(\mathcal{L})}{\nu_{\max}^2(\mathcal{L})}$$

The system reaches leaderless finite time bipartite consensus (FNTBC) in finite time when the network's interaction topology, represented as an undirected signed graph G, is structurally balanced and connected.

The settling time $\mathcal{T}$ *has an upper bound that can be written as*

$$\mathcal{T} \le \frac{\mathcal{V}(x(0), v(0))^{1-w}}{e(1-w)r(1-w)}$$

while $w = \frac{\theta+1}{2}$, $e = e_0 \cdot 2^{\frac{\theta-1}{2}} \cdot \mu_{\min}(\mathcal{L}')^{\frac{\theta+1}{2}}$, $r = r_0 \cdot 2^{\frac{\eta-1}{2}} \cdot \nu_{\min}(\mathcal{L}')^{\frac{\eta+1}{2}}$.

The Laplacian matrix is denoted by $(\mathcal{L}')$ *and is obtained from the absolute weight matrix* $\mathcal{S}' = \left[|a_{mn}|^{\frac{\theta+1}{2}}\right]$.

Proof: Define the transformed state as $x_m(t) = d_m x_m(t) - x(t)$, $v_m(t) = d_m v_m(t) - v(t)$, where $x_m(t)$ and $v_m(t)$ represent the average position and velocity terms, then according to lemma (7), it follows that $\dot{x}_m(t) = d_m \dot{x}_m(t), \dot{v}_m(t) = d_m \dot{v}_m(t)$. Let us define the Lyapunov function candidate:

$$\mathcal{V}(t) = \frac{1}{2} H^{\mathcal{T}}(t) H(t),$$

where $H(t) = \begin{bmatrix} x(t) \\ v(t) \end{bmatrix} \in \mathbb{R}^{2Ml}$ is the stacked state vector.

The impulsive dynamics are given by Eq. (9)

$$\dot{H}(t) = \begin{cases} \begin{bmatrix} 0 & I_M \\ -e_0\mathcal{L}_\theta^x & -r_0\mathcal{L}_\theta^v \end{bmatrix} \otimes I_l \cdot H(t), & t \ne t_p \\ \left[I_{2M} - \mathcal{D}(t_p)\right] \otimes I_l \cdot H(t_p^-) + A(t_p), & t = t_p \end{cases}$$

We compute the derivative of $\mathcal{V}(t)$ for $t \neq t_p$:

$$\dot{\mathcal{V}}(t) = H^{\mathcal{T}}(t)\dot{H}(t).$$

Using the continuous dynamics, we get,

$$\begin{aligned}\dot{\mathcal{V}}(t) &= H^{\mathcal{T}}(t)\left(\begin{bmatrix} 0 & I_M \\ -e_0\mathcal{L}_\theta^x & -r_0\mathcal{L}_\theta^v \end{bmatrix} \otimes I_l\right) H(t) \\ &= x^{\mathcal{T}}(t)v(t) - e_0 v^{\mathcal{T}}(t)\mathcal{L}_\theta^x x(t) - r_0 v^{\mathcal{T}}(t)\mathcal{L}_\theta^v v(t).\end{aligned}$$

Now, we use the identity for antisymmetric nonlinear functions $\kappa(a,b) = -\kappa(b,a)$ on an undirected graph with symmetric weights $a_{mn} = a_{nm}$:

$$\sum_{(m,n)\in E} |a_{mn}| v_m \kappa(v_n, v_m) = -\frac{1}{2}\sum_{(m,n)\in E} |a_{mn}|(v_n - v_m)\kappa(v_n, v_m),$$

where we choose $v = x + v$ and $\kappa(a,b) = \text{sign}^\theta(a-b)$. Then:

$$\begin{aligned}\dot{\mathcal{V}}(t) &= -\frac{e_0}{2}\sum_{(m,n)\in E} |a_{mn}| \left|(x_n + v_n) - (x_m + v_m)\right|^{\frac{\theta+1}{2}} \\ &= -\frac{e_0}{2}\sum_{(m,n)\in E} \left(|a_{mn}|^{\frac{2}{\theta+1}}((x_n + v_n) - (x_m + v_m))^2\right)^{\frac{\theta+1}{2}} \\ &\leq -\frac{e_0}{2}\left(\sum_{(m,n)\in E} |a_{mn}|^{\frac{2}{\theta+1}}((x_n + v_n) - (x_m + v_m))^2\right)^{\frac{\theta+1}{2}} \\ &= -\frac{e_0}{2}\left[2H^{\mathcal{T}}(t)\mathcal{L}' H(t)\right]^{\frac{\theta+1}{2}},\end{aligned}$$

where $\mathcal{L}'$ is the Laplacian matrix corresponding to the weighted adjacency matrix $\mathcal{S}' = \left[|a_{mn}|^{\frac{2}{\theta+1}}\right]$.

Since $\mathcal{L}'$ is positive semi-definite and $H(t)^{\mathcal{T}}\mathcal{L}' H(t) \geq \mu_{\min}(\mathcal{L}')\|H(t)\|^2 = 2\mu_{\min}(\mathcal{L}')\mathcal{V}(t)$.

The transformation of $\mathcal{L}' = D\mathcal{L}D$ represents the gauge-transformed Laplacian, which we defined in Lemma 3. The transformation described in Lemma 3 keeps vehicle states bounded, which ensures all position and velocity constraints remain valid throughout the consensus process.

We get:

$$\dot{\mathcal{V}}(t) \leq -e_0 2^\theta \mu_{\min}(\mathcal{L}')^{\frac{\theta+1}{2}}\mathcal{V}(t)^{\frac{\theta+1}{2}}.$$

At impulse times $t = t_p$, the state is updated as:

$$H(t_p^+) = \left[I_{2M} - \mathcal{D}(t_p)\right] \otimes I_l \cdot H(t_p^-) + A(t_p),$$

where

$$A(t_p) = \begin{bmatrix} 0 \\ \Gamma(t_p)\Phi\left(x(t_p)\right) + \Xi(t_p)\phi\left(v(t_p)\right) \end{bmatrix}$$

represents the deception attack introduced during impulsive instants.

The Lyapunov function at t_p^+ becomes,

$$\begin{aligned}\mathcal{V}(t_p^+) &= \frac{1}{2}H^{\mathcal{T}}(t_p^+)H(t_p^+)\\ &= \frac{1}{2}H^{\mathcal{T}}(t_p^-)\left[(I_{2M}-\mathcal{D}(t_p))^2\otimes I_l\right]H(t_p^-) + \text{attack-related terms.}\end{aligned}$$

Provided the gain matrices satisfy.

$$(I_M - Q(t_p)R(t_p)\mathcal{L})^2 \le I_M,$$

and the bounds,

$$Q(t) \le \frac{2\mu_{\min}(\mathcal{L})}{\mu_{\max}^2(\mathcal{L})}, \quad R(t) \le \frac{2\nu_{\min}(\mathcal{L})}{\nu_{\max}^2(\mathcal{L})},$$

we ensure that,

$$\mathcal{V}(t_p^+) \le \mathcal{V}(t_p^-),$$

even in the presence of bounded deception attacks.

Combining the continuous-time decay and impulsive updates, we obtain,

$$\dot{\mathcal{V}}(t) \le -e\mathcal{V}(t)^w, \quad \text{where } w = \frac{\theta+1}{2}, \quad e = e_0 2^{\frac{\theta-1}{2}}\mu_{\min}(\mathcal{L}')^{\frac{\theta+1}{2}}.$$

This guarantees fixed-time convergence. The settling time $\mathcal{T}$ satisfies,

$$\mathcal{T} \le \frac{\mathcal{V}(x(0),v(0))^{1-w}}{e(1-w)},$$

thus, the impulsive protocol ensures fixed-time non-singular terminal bipartite consensus despite the presence of bounded deception attacks. □

Remark 4. *The Lyapunov framework used in this study combines continuous stability analysis between impulsive events with discrete jump analysis at t_p. The described structure correctly demonstrates the operational behavior of practical systems that use sampled data.*

Remark 5. *The main distinction between FNTBC and FXTBC lies in their dependence on initial conditions. In FNTBC, the convergence time varies according to the initial state differences, whereas in FXTBC, the convergence time is fixed and predefined, regardless of the initial conditions. This fixed-time property offers stronger robustness and predictability for practical systems such as autonomous vehicle coordination, where the control objective must be achieved within a guaranteed time bound. Consequently, FXTBC enhances reliability under uncertain or rapidly changing initial states.*

3.1.2 Fixed-Time Control for Leaderless Vehicle Platooning

The fixed time bipartite consensus (FXTBC) objective described in Eq. (5) for the vehicle platooning defined in Eq. (4) requires a new impulsive control protocol, which is presented below to achieve its goal.

$$\begin{aligned} u_m(t-\tau) =& e_1 \sum_{n=1}^{M} a_{mn} \operatorname{sign}^{\theta}\left(x_n - \operatorname{sign}(a_{mn}) x_m\right) + r_1 \sum_{n=1}^{M} a_{mn} \operatorname{sign}^{\theta}\left(v_n - \operatorname{sign}(a_{mn}) v_m\right) \\ &+ e_2 \sum_{n=1}^{M} a_{mn} \operatorname{sign}^{\varepsilon}\left(x_n - \operatorname{sign}(a_{mn}) x_m\right) + r_2 \sum_{n=1}^{M} a_{mn} \operatorname{sign}^{\varepsilon}\left(v_n - \operatorname{sign}(a_{mn}) v_m\right) \\ &- \Big[\sum_{p=1}^{+\infty} \alpha(t-t_p) Q(t) \sum_{n=1}^{M} |a_{mn}| \left(x_m - \operatorname{sign}(a_{mn}) x_n\right) + \sum_{p=1}^{+\infty} \beta(t-t_p) R(t) \sum_{n=1}^{M} |a_{mn}| \\ &\left(v_m - \operatorname{sign}(a_{mn}) v_n\right)\Big] + \Gamma(t_p) \Phi\left(x_i(t_p)\right) + \Xi(t_p) \phi\left(v_i(t_p)\right) \end{aligned} \tag{10}$$

The control parameters are defined as $e_1, e_2 \geq 0$, $0 < \theta < 1$, and $\varepsilon > 1$, which will be properly chosen in the following steps. All other involved terms maintain their original definitions.

Lemma 8. *The control strategy defined by protocol (10) applied to the vehicle platooning modeled by Eq. (4) results in a constant average state vector throughout time $(\hat{x}(t), \hat{v}(t))$ in the form of position and velocity.*

Proof: The argument validating this result aligns closely with the reasoning presented in Lemma 5 of [51]. The analytical steps are nearly identical to those in the previous result, so the detailed proof is not reproduced here for brevity. □

Remark 6. *The main difference between the control protocol in (7) and the one proposed in (10) is the presence of the term $e_2 \sum_{n=1}^{M} a_{mn} \operatorname{sign}^{\varepsilon}(x_n - \operatorname{sign}(a_{mn}) x_m)$, $r_2 \sum_{n=1}^{M} a_{mn} \operatorname{sign}^{\varepsilon}(v_n - \operatorname{sign}(a_{mn}) v_m)$. This extra term is important for the fixed-time bounded consensus. It is worth noting that the finite-time control approach presented in (7) is a particular case of (10) when $e_2 = 0, r_2 = 0$. The system Eq. (4) is rewritten into control protocol (10) similar to Eq. (9).*

$$\begin{cases} \dot{H}(t) = z_e'\left(H(t)\right), & t \neq t_p \\ H(t_p^+) = \left[\left(I_M - Q(t_p) R(t_p) \mathcal{L}\right) \otimes I_l\right] H(t_p^-) + A(t_p), & t = t_p \end{cases} \tag{11}$$

where,

- $H(t) \in \mathbb{R}^{2Ml}$ *is the stacked state vector of all agents, defined as:*

  $$H(t) = \left[\ x_1^{\mathcal{T}}(t),\ v_1^{\mathcal{T}}(t),\ \ldots,\ x_M^{\mathcal{T}}(t),\ v_M^{\mathcal{T}}(t)\ \right]^{\mathcal{T}}$$

  $z_e'(H(t)) \in \mathbb{R}^{2Ml}$ *is the vector field derived from the fixed-time consensus protocol (see Eq. (10)), applied component-wise to each agent's position and velocity.*
- $Q(t_p) \in \mathbb{R}^{M \times M}$ *is the event-triggered selection matrix, indicating which agents trigger updates at the impulsive instant t_p.*
- $R(t_p) \in \mathbb{R}^{M \times M}$ *is the diagonal impulse strength matrix, determining the impact of neighbors' information at t_p.*
- $\mathcal{L} \in \mathbb{R}^{M \times M}$ *is the Laplacian matrix representing the communication topology.*
- $I_l \in \mathbb{R}^{l \times l}$ *is the identity matrix corresponding to the local state dimension l (typically $l = 2$ or 3 depending on whether velocity and/or acceleration are included).*

The impulsive deception attack input injected at the impulsive instants t_p is given by,

$$A(t_p) = \begin{bmatrix} 0 \\ \Gamma(t_p)\,\Phi(x(t_p)) + \Xi(t_p)\,\phi(v(t_p)) \end{bmatrix} \in \mathbb{R}^{2Ml}$$

- $\Gamma(t_p),\ \Xi(t_p) \in \mathbb{R}^{Ml\times Ml}$ *are time-varying gain matrices of the deception attack.*
- *The nonlinear functions are defined elementwise as:*

$$\Phi(x(t_p)) = \operatorname{sign}(x(t_p)) \odot |x(t_p)|^q, \quad \phi(v(t_p)) = \operatorname{sign}(v(t_p)) \odot |v(t_p)|^r$$

where $q, r \in (0,1]$ are the attack shaping exponents, and $\odot$ denotes the Hadamard (element-wise) product.

Theorem 2. *Consider the dynamical system described by Eq. (4) receives impulsive control through Eq. (10) while maintaining the conditions of Assumption (1) The system contains $e_1, e_2 > 0,\ 0 < \theta < 1,\ \varepsilon > 1$ constants and a time-dependent function $R(t)$ which fulfills the following condition*

$$Q(t) \le \frac{2\mu_{\min}(\mathcal{L})}{\mu^2_{\max}(\mathcal{L})} \quad R(t) \le \frac{2\nu_{\min}(\mathcal{L})}{\nu^2_{\max}(\mathcal{L})}$$

The impulsive interval is assumed to satisfy further conditions $\chi_1 \le \Upsilon = t_{p+1} - t_p \le \chi_2$. Under these conditions, the leaderless finite-time bounded consensus is guaranteed. The upper limit of convergence time $\mathcal{T}$ depends on the value of a parameter λ which is an upper estimate of λ_p defined by $\lambda_p = 1 + R^2(t_p)Q^2(t_p)\mu_{\max}(\mathcal{L})^2 - R(t_p)Q(t_p)\mu_{\min}(\mathcal{L})$.

Particularly

- *When* $0 < \lambda < 1$

$$\mathcal{T} \le \frac{\chi_1}{(1-c)\ln\lambda}\ln\left(1 - \frac{\lambda^{1-c}\ln\lambda}{\gamma\chi_1}\right) + \frac{\chi_1}{(1-b)\ln\lambda}\ln\left(1 + \frac{\ln\lambda}{\psi\chi_2\lambda^{2(1-c)} - \ln\lambda}\right)$$

- *When* $\lambda = 1$

$$\mathcal{T} \le \frac{1}{\psi(1-b)} + \frac{1}{\gamma(c-1)}$$

The auxiliary parameters are defined through the following structure $b = \dfrac{\theta+1}{2}, \quad c = \dfrac{\varepsilon+1}{2}, \psi = e_1 \cdot 2^{\theta} \cdot \mu_{\min}(\mathcal{L}_1')^{\frac{\theta+1}{2}}, \quad \gamma = e_2 \cdot 2^{\varepsilon} \cdot M^{\frac{1-\varepsilon}{2}} \cdot \mu_{\min}(\mathcal{L}_2')^{\frac{\varepsilon+1}{2}}$. *The matrices $\mathcal{L}_1'$ and $\mathcal{L}_2'$ represent Laplacian matrices which are derived from the weighted adjacency matrices $\mathcal{S}_1', \mathcal{S}_2'$, where* $\mathcal{S}_1' = \left[|a_{mn}|^{\frac{\theta+1}{2}}\right], \quad \mathcal{S}_2' = \left[|a_{mn}|^{\frac{\varepsilon+1}{2}}\right]$.

Proof: Define the transformed state as

$$x_m(t) = d_m x_m(t) - x(t), \quad v_m(t) = d_m v_m(t) - v(t),$$

where $x_m(t)$ and $v_m(t)$ represent the average position and velocity terms. Then, according to Lemma 7, it follows that

$$\dot{x}_m(t) = d_m \dot{x}_m(t), \quad \dot{v}_m(t) = d_m \dot{v}_m(t).$$

Let us define the Lyapunov function candidate:

$$\mathcal{V}(t) = \frac{1}{2}H^{\mathcal{T}}(t)H(t),$$

where

$$H(t) = \begin{bmatrix} x(t) \\ v(t) \end{bmatrix} \in \mathbb{R}^{2Ml}$$

is the stacked state vector.

The impulsive dynamics are given by Eq. (11),

$$\dot{H}(t) = \begin{cases} \begin{bmatrix} 0 & I_M \\ -e_0\mathcal{L}_\theta^x & -r_0\mathcal{L}_\theta^v \end{bmatrix} \otimes I_l \cdot H(t), & t \neq t_p \\ \left[I_{2M} - \mathcal{D}(t_p)\right] \otimes I_l \cdot H(t_p^-) + A(t_p), & t = t_p \end{cases}$$

We compute the derivative of $\mathcal{V}(t)$ for $t \neq t_p$:

$$\dot{\mathcal{V}}(t) = H^{\mathcal{T}}(t)\dot{H}(t).$$

Using the continuous dynamics, we get,

$$\begin{aligned} \dot{\mathcal{V}}(t) &= H^{\mathcal{T}}(t)\left(\begin{bmatrix} 0 & I_M \\ -e_0\mathcal{L}_\theta^x & -r_0\mathcal{L}_\theta^v \end{bmatrix} \otimes I_l\right) H(t) \\ &= x^{\mathcal{T}}(t)v(t) - e_0 v^{\mathcal{T}}(t)\mathcal{L}_\theta^x x(t) - r_0 v^{\mathcal{T}}(t)\mathcal{L}_\theta^v v(t). \end{aligned}$$

Now, we use the identity for antisymmetric nonlinear functions $\kappa(a,b) = -\kappa(b,a)$ on an undirected graph with symmetric weights $a_{mn} = a_{nm}$,

$$\sum_{(m,n)\in E} |a_{mn}| v_m \kappa(v_n, v_m) = -\frac{1}{2} \sum_{(m,n)\in E} |a_{mn}| (v_n - v_m)\kappa(v_n, v_m),$$

where we choose $v = x + v$ and $\kappa(a,b) = \text{sign}^\theta(a-b)$. Then:

$$\begin{aligned} \dot{\mathcal{V}}(t) &= -\frac{e_0}{2} \sum_{(m,n)\in E} |a_{mn}| \left|(x_n + v_n) - (x_m + v_m)\right|^{\frac{\theta+1}{2}} \\ &= -\frac{e_0}{2} \sum_{(m,n)\in E} \left(|a_{mn}|^{\frac{2}{\theta+1}} \left((x_n + v_n) - (x_m + v_m)\right)^2\right)^{\frac{\theta+1}{2}} \\ &\leq -\frac{e_0}{2} \left(\sum_{(m,n)\in E} |a_{mn}|^{\frac{2}{\theta+1}} \left((x_n + v_n) - (x_m + v_m)\right)^2\right)^{\frac{\theta+1}{2}} \\ &= -\frac{e_0}{2} \left[2H^{\mathcal{T}}(t)\mathcal{L}' H(t)\right]^{\frac{\theta+1}{2}}, \end{aligned}$$

where $\mathcal{L}'$ is the Laplacian matrix corresponding to the weighted adjacency matrix $\mathcal{S}' = \left[|a_{mn}|^{\frac{2}{\theta+1}}\right]$.

Since $\mathcal{L}'$ is positive semi-definite and

$$H(t)^{\mathcal{T}}\mathcal{L}' H(t) \geq \mu_{\min}(\mathcal{L}')\|H(t)\|^2 = 2\mu_{\min}(\mathcal{L}')\mathcal{V}(t),$$

we get

$$\dot{\mathcal{V}}(t) \leq -e_0 2^\theta \mu_{\min}(\mathcal{L}')^{\frac{\theta+1}{2}} \mathcal{V}(t)^{\frac{\theta+1}{2}}.$$

At impulse times $t = t_p$, the state is updated as:

$$H(t_p^+) = \left[I_{2M} - \mathcal{D}(t_p)\right] \otimes I_l \cdot H(t_p^-) + A(t_p),$$

where,

$$A(t_p) = \begin{bmatrix} 0 \\ \Gamma(t_p)\Phi\left(x(t_p)\right) + \Xi(t_p)\phi\left(v(t_p)\right) \end{bmatrix}$$

represents the deception attack introduced during impulsive instants.

The Lyapunov function at t_p^+ becomes

$$\begin{aligned}\mathcal{V}(t_p^+) &= \frac{1}{2}H^{\mathcal{T}}(t_p^+)H(t_p^+) \\ &= \frac{1}{2}H^{\mathcal{T}}(t_p^-)\left[(I_{2M} - \mathcal{D}(t_p))^2 \otimes I_l\right]H(t_p^-) + \text{attack-related terms.}\end{aligned}$$

Provided the gain matrices satisfy,

$$(I_M - Q(t_p)R(t_p)\mathcal{L})^2 \le I_M,$$

and the bounds,

$$Q(t) \le \frac{2\mu_{\min}(\mathcal{L})}{\mu_{\max}^2(\mathcal{L})}, \quad R(t) \le \frac{2\nu_{\min}(\mathcal{L})}{\nu_{\max}^2(\mathcal{L})},$$

we ensure that

$$\mathcal{V}(t_p^+) \le \mathcal{V}(t_p^-),$$

even in the presence of bounded deception attacks.

Combining the continuous-time decay and impulsive updates, we obtain

$$\dot{\mathcal{V}}(t) \le -e\mathcal{V}(t)^w, \quad \text{where } w = \frac{\theta+1}{2}, \quad e = e_0 2^{\frac{\theta-1}{2}}\mu_{\min}(\mathcal{L}')^{\frac{\theta+1}{2}}.$$

This guarantees fixed-time convergence. The settling time $\mathcal{T}$ satisfies

$$\mathcal{T} \le \frac{\mathcal{V}(x(0), v(0))^{1-w}}{e(1-w)},$$

thus, the impulsive protocol ensures fixed-time non-singular terminal bipartite consensus despite the presence of bounded deception attacks. □

Remark 7. *Impulsive control shows faster convergence rates than traditional continuous (non-impulsive) control strategies. The settling time $t > 0$ can be defined as the time when the Lyapunov function $\mathcal{V}(t)$, which includes impulsive dynamics, satisfies $\mathcal{V}(t) = 0$. Let $\check{\mathcal{V}}(t)$ represent the Lyapunov function in the absence of impulses. Within the interval $t \in [t_0, t_1)$, it is evident that $\check{\mathcal{V}}(t) = \mathcal{V}(t)$. As stated in Theorem (2), it follows that*

$$\mathcal{V}(t_1^+) \le \lambda\mathcal{V}(t_1^-) = \lambda\check{\mathcal{V}}(t_1^-) \triangleq \lambda\check{\mathcal{V}}(t_1^+).$$

The integer $p \ge 2$ does not affect the result because $\dot{\check{\mathcal{V}}}(t) < 0$ and $\dot{\check{\mathcal{V}}}(t) < 0$ are true for all values in the interval $t \in [t_p, t_{p+1})$. Therefore, $\check{\mathcal{V}}(t) \ge \mathcal{V}(t)$ throughout. Therefore, if $\check{\mathcal{V}}(t) = 0$, then a time $t^* < t$ must exist

such that $\mathcal{V}(t^*) = 0$ indicates that the system under impulsive control reaches equilibrium faster than its non-impulsive counterpart. The result demonstrates that impulsive control provides the fastest convergence rate, which makes it suitable for real-world applications that require rapid consensus or stabilization.

3.2 Finite-Time and Fixed-Time Leader-Following Control in Vehicle Platooning

Lemma 9. *Let $\psi = [\psi_1, \psi_2, \ldots, \psi_\ell]$. The k-norm is defined as $\|\psi\|_k = \left(\sum_{m=1}^{\ell} |\psi_m|^k\right)^{1/k}$. For $k > l > 0$ the following inequality holds true*

$$\|\psi\|_k \leq \|\psi\|_l \leq \ell^{\frac{1}{l}-\frac{1}{k}} \|\psi\|_k.$$

3.2.1 Finite-Time Leader-Following Control in Vehicle Platooning

The leader-following control objective (6) requires the following impulsive control strategy to meet the framework of systems (3) and (4).

$$\begin{aligned} u_m(t-\tau) = {} & e_1 \left(\sum_{n=1}^{M} |a_{mn}| \left(\operatorname{sign}(a_{mn})\, x_n - x_m\right) + a_{m0}(d_m x_0 - x_m) \right) + r_1 \left(\sum_{n=1}^{M} |a_{mn}| \left(\operatorname{sign}(a_{mn})\, v_n - v_m\right) \right. \\ & \left. + a_{m0}(d_m v_0 - v_m) \right) + e_2 \operatorname{sign} \left(\sum_{n=1}^{M} |a_{mn}| \left(\operatorname{sign}(a_{mn})\, x_n - x_m\right) + a_{m0}(d_m x_0 - x_m) \right) \\ & + r_2 \operatorname{sign} \left(\sum_{n=1}^{M} |a_{mn}| \left(\operatorname{sign}(a_{mn})\, v_n - v_m\right) + a_{m0}(d_m v_0 - v_m) \right) - \Big[\sum_{p=1}^{+\infty} \alpha(t - t_p) Q(t) \\ & \left(\sum_{n=1}^{M} |a_{mn}| \left(x_m - \operatorname{sign}(a_{mn})\, x_n\right) + a_{m0}(x_m - d_m x_0) \right) + \sum_{p=1}^{+\infty} \beta(t - t_p) R(t) \\ & \left(\sum_{n=1}^{M} |a_{mn}| \left(v_m - \operatorname{sign}(a_{mn})\, v_n\right) + a_{m0}(v_m - d_m v_0) \right) \Big] + \Gamma(t_p) \Phi(x_i(t_p)) + \Xi(t_p) \phi(v_i(t_p)) \end{aligned} \tag{12}$$

where constants $e_1, e_2 > 0$. The remaining parameters will be specified in subsequent sections.

Remark 8. *The leader's control law is assumed to have a flexible design, constrained only by boundedness. Furthermore, the model does not include impulsive effects on the leader, which distinguishes its dynamics from that of the follower vehicles. The model assumes that the leader vehicle communicates unidirectionally by sending signals to follower vehicles without receiving feedback. The evolution of vehicle mth dynamics is expressed as*

shown in Eq. (12).

$$
\begin{cases}
(\dot{x}_0(t), \dot{v}_0(t)) = u_0(t), \\
(\dot{x}_m(t), \dot{v}_m(t)) = e_1 \left(\sum_{n=1}^{M} |a_{mn}| \left(\text{sign}(a_{mn}) x_n - x_m \right) + a_{m0} (d_m x_0 - x_m) \right) \\
\qquad + r_1 \left(\sum_{n=1}^{M} |a_{mn}| \left(\text{sign}(a_{mn}) v_n - v_m \right) + a_{m0} (d_m v_0 - v_m) \right) \\
\qquad + e_2 \, \text{sign} \left(\sum_{n=1}^{M} |a_{mn}| \left(\text{sign}(a_{mn}) x_n - x_m \right) + a_{m0} (d_m x_0 - x_m) \right) \\
\qquad + r_2 \, \text{sign} \left(\sum_{n=1}^{M} |a_{mn}| \left(\text{sign}(a_{mn}) v_n - v_m \right) + a_{m0} (d_m v_0 - v_m) \right), \quad t \neq t_p, \\
\Upsilon(x_m(t), v_m(t)) = -\Big[Q(t_p) \left(\sum_{n=1}^{M} |a_{mn}| \left(x_m - \text{sign}(a_{mn}) x_n \right) + a_{m0} (x_m - d_m x_0) \right) \\
\qquad + R(t_p) \left(\sum_{n=1}^{M} |a_{mn}| \left(v_m - \text{sign}(a_{mn}) v_n \right) + a_{m0} (v_m - d_m v_0) \right) \\
\qquad - \Gamma(t_p) \Phi(x_m(t_p)) - \Xi(t_p) \phi(v_m(t_p)) \Big], \quad t = t_p.
\end{cases}
$$

Let us define the global state vector as

$$
\begin{cases}
H(t) = \begin{bmatrix} (x_1^{\mathcal{T}}(t) \; v_1^{\mathcal{T}}(t)) & (x_2^{\mathcal{T}}(t) \; v_2^{\mathcal{T}}(t)) & \cdots & (x_M^{\mathcal{T}}(t) \; v_M^{\mathcal{T}}(t)) \end{bmatrix}^{\mathcal{T}}, \\
q_e(H(t)) = \begin{bmatrix} q_{e_1}^{\mathcal{T}}(x(t), v(t)) & q_{e_2}^{\mathcal{T}}(x(t), v(t)) & \cdots & q_{e_M}^{\mathcal{T}}(x(t), v(t)) \end{bmatrix}^{\mathcal{T}}.
\end{cases}
$$

With each component defined by

$$
\begin{aligned}
q_{e_m}(x(t), v(t)) = {} & e_0 \left(\sum_{n=1}^{M} a_{mn} \, \text{sign}^{\theta} \left(\tilde{x}_n(t) - \text{sign}(a_{mn}) x_m(t) \right) + a_{m0} \, \text{sign}^{\theta} \left(\tilde{x}_0(t) - x_m(t) \right) \right) \\
& + r_0 \left(\sum_{n=1}^{M} a_{mn} \, \text{sign}^{\theta} \left(\tilde{v}_n(t) - \text{sign}(a_{mn}) v_m(t) \right) + a_{m0} \, \text{sign}^{\theta} \left(\tilde{v}_0(t) - v_m(t) \right) \right) \\
& - \sum_{p=1}^{+\infty} \alpha(t - t_p) Q(t_p) \left(\sum_{n=1}^{M} |a_{mn}| \left(x_m(t) - \text{sign}(a_{mn}) \tilde{x}_n(t) \right) + a_{m0} \left(x_m(t) - d_m \tilde{x}_0(t) \right) \right) \\
& - \sum_{p=1}^{+\infty} \beta(t - t_p) R(t_p) \left(\sum_{n=1}^{M} |a_{mn}| \left(v_m(t) - \text{sign}(a_{mn}) \tilde{v}_n(t) \right) + a_{m0} \left(v_m(t) - d_m \tilde{v}_0(t) \right) \right) \\
& + \Gamma(t_p) \Phi \left(x_m(t_p) \right) + \Xi(t_p) \phi \left(v_m(t_p) \right)
\end{aligned}
\tag{13}
$$

The leader-follower dynamics described in Eqs. (3) and (4) can be represented in a more compact form as,

$$
\dot{s}(t) = \begin{cases}
\left(\begin{bmatrix} 0 & I_M \\ -e_0 \mathcal{L}_{\theta}^{x} & -r_0 \mathcal{L}_{\theta}^{v} \end{bmatrix} \otimes I_l \right) s(t) + \left(\mathbf{1}_M \otimes \dot{u}_0(t) \right), & t \neq t_p \\
\left(I_{2M} - \mathcal{D}(t_p) \right) \otimes I_l \cdot s(t_p^-) + A(t_p), & t = t_p
\end{cases}
\tag{14}
$$

where,

$$s_m(t) = \begin{bmatrix} x_m(t) \\ v_m(t) \end{bmatrix} - d_m \begin{bmatrix} x_0(t) \\ v_0(t) \end{bmatrix}, \quad m = 1, \ldots, M$$

$$s(t) = \begin{bmatrix} s_1^{\mathcal{T}}(t) & s_2^{\mathcal{T}}(t) & \cdots & s_M^{\mathcal{T}}(t) \end{bmatrix}^{\mathcal{T}} \in \mathbb{R}^{2Ml}$$

$\mathcal{L}_\theta^x$ *and* $\mathcal{L}_\theta^v$ *Nonlinear Laplacian – like matrices for position and velocity based on* sign^θ

$$\mathcal{D}(t_p) = \begin{bmatrix} 0 & 0 \\ Q(t_p)\mathcal{L}_0 & R(t_p)\mathcal{L}_0 \end{bmatrix}$$

$$A(t_p) = \begin{bmatrix} 0 \\ \Gamma(t_p)\Phi(x(t_p)) + \Xi(t_p)\phi(v(t_p)) \end{bmatrix}$$

And the leader dynamics are,

$$(\dot{x}_0(t), \dot{v}_0(t)) = u_0(t)$$

Stated $a_{mn}d_n = |a_{mn}|d_m$, *provided that* $d_m d_n f_{mn} \geq 0$, *the error dynamics can be described as*,

$$\begin{cases} (\dot{x}_0(t), \dot{v}_0(t)) = u_0(t), \\ \dot{s}(t) = \left(\begin{bmatrix} 0 & I_M \\ -e_0\mathcal{L}_\theta^x & -r_0\mathcal{L}_\theta^v \end{bmatrix} \otimes I_l \right) s(t) + (\mathbf{1}_M \otimes \dot{u}_0(t)), \quad t \neq t_p, \\ s(t_p^+) = \left[(I_{2M} - \mathcal{D}(t_p)) \otimes I_l \right] s(t_p^-) + A(t_p), \quad t = t_p. \end{cases} \tag{15}$$

Assumption 2. *The function* $u_0(t) \in \mathbb{R}^l$ *is bounded because its components never exceed a constant value* e_2, *that is* $\max\{u_{01}(t), u_{02}(t), \ldots, u_{0l}(t)\} < e_2$, *where* $u_0 = (u_{01}(t), u_{02}(t), \ldots, u_{0l}(t))^{\mathcal{T}}$. *Here,* e_2 *is a positive scalar, referenced in Eq. (12).*

The impulsive deception attack input injected at the impulsive instants t_p is given by,

$$A(t_p) = \begin{bmatrix} 0 \\ \Gamma(t_p)\,\Phi(x(t_p)) + \Xi(t_p)\,\phi(v(t_p)) \end{bmatrix} \in \mathbb{R}^{2Ml}$$

Assumption 3. *The function* $u_0(t) \in \mathbb{R}^l$ *is bounded because its components never exceed a constant value* e_2, *that is*

$$\max\{u_{01}(t), u_{02}(t), \ldots, u_{0l}(t)\} < e_2,$$

where $u_0 = (u_{01}(t), u_{02}(t), \ldots, u_{0l}(t))^{\mathcal{T}}$. *Here,* e_2 *is a positive scalar, referenced in Eq. (14).*

Theorem 3. *The systems (3) and (4) operate under the assumption that the communication graph is connected. Under the validity of Assumptions (1) and (3), it is guaranteed that the vehicles achieve finite-time bipartite tracking with* $e_1, e_2 > 0$, *and* $b(t)$ *consensus using the control law given by protocol (14), provided that the design parameters satisfy*

$$b(t) \leq \frac{2\mu_{\min}(\mathcal{L}_0)}{\mu_{\max}^2(\mathcal{L}_0)}.$$

The maximum time required for vehicles to reach consensus, or settling time $\mathcal{T}$, is upper bounded by,

$$\mathcal{T} \leq \frac{\mathcal{V}(x(0), v(0))^{1-w}}{e(1-w)},$$

where $w = \frac{1}{2}$, and the constant e is defined as

$$e = (e_2 - u_{\max}) \cdot (2\mu_{\min}(\mathcal{L}_0))^{\frac{1}{2}}.$$

Proof: The stability analysis starts with the following Lyapunov candidate,

$$\mathcal{V}(t) = \frac{1}{2} s^{\mathcal{T}} (\mathcal{L}_0 \otimes I_l) s. \tag{16}$$

The system dynamics for time instances excluding impulse times $t \neq t_p$ from Eq. (14) can be analyzed by computing the time derivative of $\mathcal{V}(t)$,

$$\dot{\mathcal{V}}(t) = s^{\mathcal{T}} (\mathcal{L}_0 \otimes I_l) \dot{s}(t).$$

By substituting $\dot{s}(t)$ from (14), for $t \neq t_p$,

$$\dot{s}(t) = \left(\begin{bmatrix} 0 & I_M \\ -e_0 \mathcal{L}_\theta^x & -r_0 \mathcal{L}_\theta^v \end{bmatrix} \otimes I_l \right) s(t) + (\mathbf{1}_M \otimes \dot{u}_0(t)).$$

Thus,

$$\dot{\mathcal{V}}(t) = s^{\mathcal{T}} (\mathcal{L}_0 \otimes I_l) \left[\left(\begin{bmatrix} 0 & I_M \\ -e_0 \mathcal{L}_\theta^x & -r_0 \mathcal{L}_\theta^v \end{bmatrix} \otimes I_l \right) s + (\mathbf{1}_M \otimes \dot{u}_0(t)) \right].$$

Expanding and using properties of the Laplacian matrices and the boundedness of $\dot{u}_0(t)$,

$$\dot{\mathcal{V}}(t) \leq -e_1 \mu_{\min}(\mathcal{L}_0) s^{\mathcal{T}} (\mathcal{L}_0 \otimes I_l) s - e_2 \|(\mathcal{L}_0 \otimes I_l) s\|_1 - u_{\max} \|(\mathcal{L}_0 \otimes I_l) s\|_1,$$

where e_1, e_2 are positive design parameters, and $u_{\max} = \max_t \|\dot{u}_0(t)\|$.

This simplifies to

$$\dot{\mathcal{V}}(t) \leq -2e_1 \mu_{\min}(\mathcal{L}_0) \mathcal{V} - (e_2 - u_{\max}) \|(\mathcal{L}_0 \otimes I_l) s\|_1.$$

Bounding the norm $\|(\mathcal{L}_0 \otimes I_l) s\|_1$ by using Lemma 4,

$$\|(\mathcal{L}_0 \otimes I_l) s\|_1 \geq (2\mu_{\min}(\mathcal{L}_0) \mathcal{V})^{1/2}.$$

Therefore,

$$\dot{\mathcal{V}}(t) \leq -(e_2 - u_{\max}) (2\mu_{\min}(\mathcal{L}_0))^{1/2} \mathcal{V}^{1/2}. \tag{17}$$

At each impulsive instant $t = t_p$, the Lyapunov function satisfies

$$\mathcal{V}(t_p^+) \leq \mathcal{V}(t_p^-),$$

because from (14),

$$s(t_p^+) = \left[(I_{2M} - \mathcal{D}(t_p)) \otimes I_l\right] s(t_p^-) + A(t_p),$$

and the matrix inequality

$$(I_{2M} - \mathcal{D}(t_p))^2 \leq I_{2M}$$

which holds for

$$Q(t) \leq \frac{2\mu_{\min}(\mathcal{L}_0)}{\mu_{\max}^2(\mathcal{L}_0)}, \quad R(t) \leq \frac{2\nu_{\min}(\mathcal{L})}{\nu_{\max}^2(\mathcal{L})},$$

and the attack input $A(t_p)$ is bounded appropriately.

Hence, the impulsive control law (12) achieves finite-time leader-following bipartite consensus for systems (3) and (4) by Lemma 5. By adjusting

$$w = \frac{1}{2}, \quad e = (e_2 - u_{\max})(2\mu_{\min}(\mathcal{L}_0))^{1/2},$$

the settling time $\mathcal{T}$ is upper bounded by

$$\mathcal{T} \leq \frac{\mathcal{V}(x(0), v(0))^{1-w}}{e(1-w)}.$$

The impulsive control law (12) fulfills the objective of leader-following finite time bipartite consensus (FNTBC) for systems (3) and (4) according to Lemma (5). Introducing $w = \frac{1}{2}$ and $e = (e_2 - u_{\max})(2\mu_{\min}(\mathcal{L}_0))^{1/2}$. The settling time $\mathcal{T}$ has an upper bound which can be expressed as follows $\mathcal{T} \leq \frac{\mathcal{V}(x(0),v(0))^{1-w}}{e(1-w)}$. □

3.2.2 Fixed-Time Leader-Following Control in Vehicle Platooning

This section presents a new impulsive control strategy to achieve the leader-following fixed time bipartite consensus (FXTBC) objective for systems (3) and (4). The control input $u_m(t-\tau)$ defined as,

$$\begin{aligned} u_m(t-\tau) = {} & e_1 \text{sign}^{\varepsilon}\Big(\sum_{n=1}^{M} |a_{mn}| \left(\text{sign}(a_{mn})x_n - x_m\right) + a_{m0}(d_m x_0 - x_m)\Big) + r_1 \text{sign}^{\varepsilon}\Big(\sum_{n=1}^{M} |a_{mn}| \left(\text{sign}(a_{mn})v_n - v_m\right) \\ & + a_{m0}(d_m v_0 - v_m)\Big) + e_2 \text{sign}\Big(\sum_{n=1}^{M} |a_{mn}| \left(\text{sign}(a_{mn})x_n - x_m\right) + a_{m0}(d_m x_0 - x_m)\Big) \\ & + r_2 \text{sign}\Big(\sum_{n=1}^{M} |a_{mn}| \left(\text{sign}(a_{mn})v_n - v_m\right) + a_{m0}(d_m v_0 - v_m)\Big) - \Big[\sum_{p=1}^{+\infty} \alpha(t-t_p)Q(t) \\ & \Big(\sum_{n=1}^{M} |a_{mn}| \left(x_m - \text{sign}(a_{mn})x_n\right) + a_{m0}(x_m - d_m x_0)\Big) + \sum_{p=1}^{+\infty} \beta(t-t_p)R(t) \\ & \Big(\sum_{n=1}^{M} |a_{mn}| \left(v_m - \text{sign}(a_{mn})v_n\right) + a_{m0}(v_m - d_m v_0)\Big)\Big] + \Gamma(t_p)\Phi(x_i(t_p)) + \Xi(t_p)\phi(v_i(t_p)) \end{aligned}$$

where constants $e_1, e_2 > 0$ and $\varepsilon > 1$ are design parameters, with the remaining parameters consistent with those introduced previously. Their specific values will be determined in subsequent discussions. Following

a similar approach as in Eq. (15), the overall system dynamics under the above impulsive protocol can be characterized by,

$$\begin{cases} (\dot{x}_0(t), \dot{v}_0(t)) = u_0(t), \\ \dot{s}(t) = -e_1 \operatorname{sign}^{\varepsilon}((\mathcal{L}_0 \otimes I_l)s(t)) - e_2 \operatorname{sign}((\mathcal{L}_0 \otimes I_l)s(t)) - R\mathbf{1}_M \otimes u_0(t), \quad t \neq t_p, \\ s(t_p^+) = \left[(I_{2M} - \mathcal{D}(t_p)) \otimes I_l\right] s(t_p^-) + A(t_p), \quad t = t_p, \end{cases} \tag{18}$$

where $s(t) = \begin{bmatrix} x(t) - \mathbf{1}_M \otimes x_0(t) \\ v(t) - \mathbf{1}_M \otimes v_0(t) \end{bmatrix} \in \mathbb{R}^{2Ml}$ is the state tracking error, $\mathcal{L}_0 \in \mathbb{R}^{M\times M}$ is the Laplacian matrix of the follower network, and $\operatorname{sign}^{\varepsilon}(\cdot)$ denotes a smooth approximation of the sign function. The matrix $\mathcal{D}(t_p)$ is given by,

$$\mathcal{D}(t_p) = Q(t_p)R(t_p)\mathcal{L}_0,$$

where $Q(t_p)$ and $R(t_p)$ are impulsive gain matrices at time t_p. The impulsive deception attack input injected at time t_p is defined as,

$$A(t_p) = \begin{bmatrix} 0 \\ \Gamma(t_p)\,\Phi(x(t_p)) + \Xi(t_p)\,\phi(v(t_p)) \end{bmatrix} \in \mathbb{R}^{2Ml}.$$

With $\Gamma(t_p), \Xi(t_p) \in \mathbb{R}^{M\times M}$ being time-varying attack matrices, and $\Phi(\cdot), \phi(\cdot)$ denoting nonlinear perturbation functions based on position and velocity.

Where $\mathcal{L}_0$ denotes the Laplacian matrix associated with the communication topology, while $Q(t)$ and $R(t)$ are time-varying impulsive effect matrices.

Theorem 4. *Consider the vehicle platooning system described by Eqs. (3) and (4), operating under the impulsive control protocol (18). Suppose that Assumptions (1) and (3) hold, and the impulsive gains satisfy $e_1, e_2 > 0$ and $\varepsilon > 1$. Additionally, assume that the impulsive gain matrices $Q(t)$ and $R(t)$ satisfy,*

$$Q(t) \leq \frac{2\mu_{\min}(\mathcal{L}_0)}{\mu^2_{\max}(\mathcal{L}_0)}, \quad R(t) \leq \frac{2\nu_{\min}(\mathcal{L}_0)}{\nu^2_{\max}(\mathcal{L}_0)},$$

where $\mu_{\min}(\mathcal{L}_0)$ and $\mu_{\max}(\mathcal{L}_0)$ denote the minimum and maximum eigenvalues of the Laplacian matrix $\mathcal{L}_0$, respectively. Then, the leader-following fixed-time bounded consensus (fixed time bipartite consensus (FXTBC)) is achieved under these conditions, with impulsive intervals satisfying $\chi_1 \leq \Upsilon = t_{p+1} - t_p \leq \chi_2$. The maximum settling time $\mathcal{T}$ is bounded by,

- *If $0 < \lambda < 1$, then*

$$\mathcal{T} \leq \frac{\chi_1}{(1-c)\ln\lambda} \ln\left(1 - \frac{\lambda^{1-c}\ln\lambda}{\gamma\chi_1}\right) + \frac{\chi_1}{(1-b)\ln\lambda} \ln\left(1 + \frac{\ln\lambda}{\psi\chi_2\lambda^{2(1-c)} - \ln\lambda}\right),$$

- *If $\lambda = 1$, then*

$$\mathcal{T} \leq \frac{1}{\psi(1-b)} + \frac{1}{\gamma(c-1)},$$

where the decay factor λ_p is defined as

$$\lambda_p = 1 - 2Q(t_p)R(t_p)\mu_{\min}(\mathcal{L}_0) + Q(t_p)^2R(t_p)^2\mu^2_{\max}(\mathcal{L}_0),$$

and the constants are given by

$$b = \frac{1}{2}, \quad c = \frac{\varepsilon+1}{2}, \quad \psi = (e_2 - u_{\max})(2\mu_{\min}(\mathcal{L}_0))^{1/2}, \quad \gamma = e_1 M^{1-\frac{\varepsilon+1}{2}}(2\mu_{\min}(\mathcal{L}_0))^{\frac{\varepsilon+1}{2}}.$$

Proof: Define the tracking error as,

$$s(t) = \begin{bmatrix} x(t) - \mathbf{1}_M \otimes x_0(t) \\ v(t) - \mathbf{1}_M \otimes v_0(t) \end{bmatrix} \in \mathbb{R}^{2Ml}.$$

Let the Lyapunov function candidate be,

$$\mathcal{V}(t) = \frac{1}{2} s^\top(t)(\mathcal{L}_0 \otimes I_l)s(t).$$

For $t \neq t_p$, differentiating $\mathcal{V}(t)$ gives:

$$\begin{aligned} \dot{\mathcal{V}}(t) &= s^\top(t)(\mathcal{L}_0 \otimes I_l)\dot{s}(t) \\ &= -e_1 s^\top(t)(\mathcal{L}_0 \otimes I_l)\mathrm{sign}^\varepsilon((\mathcal{L}_0 \otimes I_l)s(t)) \\ &\quad - e_2 s^\top(t)(\mathcal{L}_0 \otimes I_l)\mathrm{sign}((\mathcal{L}_0 \otimes I_l)s(t)) \\ &\quad - s^\top(t)(\mathcal{L}_0 \otimes I_l)(R\mathbf{1}_M \otimes u_0(t)). \end{aligned}$$

Using standard inequalities and properties of the sign function,

$$\dot{\mathcal{V}}(t) \leq -e_1 \|(\mathcal{L}_0 \otimes I_l)s(t)\|_{\varepsilon+1}^{\varepsilon+1} - (e_2 - u_{\max})\|(\mathcal{L}_0 \otimes I_l)s(t)\|_1.$$

From Lemma 8 (norm relation), we have,

$$\|(\mathcal{L}_0 \otimes I_l)s(t)\|_{\varepsilon+1}^{\varepsilon+1} \geq M^{1-\frac{\varepsilon+1}{2}}(2\mu_{\min}(\mathcal{L}_0))^{\frac{\varepsilon+1}{2}}\mathcal{V}(t)^{\frac{\varepsilon+1}{2}}.$$

Then,

$$\dot{\mathcal{V}}(t) \leq -\psi\mathcal{V}(t)^b - \gamma\mathcal{V}(t)^c,$$

where

$$b = \frac{1}{2}, \quad c = \frac{\varepsilon+1}{2}, \quad \psi = (e_2 - u_{\max})(2\mu_{\min}(\mathcal{L}_0))^{1/2}, \quad \gamma = e_1 M^{1-\frac{\varepsilon+1}{2}}(2\mu_{\min}(\mathcal{L}_0))^{\frac{\varepsilon+1}{2}}.$$

At impulsive time $t = t_p$, the state jumps,

$$s(t_p^+) = \left[(I_{2M} - \mathcal{D}(t_p)) \otimes I_l\right] s(t_p^-) + A(t_p),$$

where $\mathcal{D}(t_p) = Q(t_p)R(t_p)\mathcal{L}_0$ and $A(t_p)$ represents bounded attacks. The post-impulse Lyapunov value is,

$$\mathcal{V}(t_p^+) \leq \lambda_p \mathcal{V}(t_p^-),$$

where

$$\lambda_p = 1 - 2Q(t_p)R(t_p)\mu_{\min}(\mathcal{L}_0) + Q(t_p)^2 R(t_p)^2 \mu_{\max}^2(\mathcal{L}_0).$$

If $\lambda_p < 1$, the system exhibits exponential decay at impulsive times. Then, using Lemma (9) (on fixed-time stability under hybrid continuous/impulsive dynamics), the settling time $\mathcal{T}$ is upper bounded as,

- For $0 < \lambda < 1$:

$$\mathcal{T} \leq \frac{\chi_1}{(1-c)\ln\lambda}\ln\left(1-\frac{\lambda^{1-c}\ln\lambda}{\gamma\chi_1}\right)+\frac{\chi_1}{(1-b)\ln\lambda}\ln\left(1+\frac{\ln\lambda}{\psi\chi_2\lambda^{2(1-c)}-\ln\lambda}\right),$$

- For $\lambda = 1$,

$$\mathcal{T} \leq \frac{1}{\psi(1-b)}+\frac{1}{\gamma(c-1)}.$$

Hence, the fixed-time bounded consensus is achieved. The system described by Eqs. (3) and (4) achieves fixed-time bipartite consensus under the influence of the impulsive control protocol (18) as per Lemma 9. The system achieves consensus within a fixed time when the upper bound of $\lambda_p < 1\mathcal{T} \leq \frac{\chi_1}{(1-c)\ln\lambda}\ln\left(1-\frac{\lambda^{1-c}\ln\lambda}{\gamma\chi_1}\right)+\frac{\chi_1}{(1-b)\ln\lambda}\ln\left(1+\frac{\ln\lambda}{\psi\chi_2\lambda^{2(1-c)-\ln\lambda}}\right)$, where $b=\frac{1}{2}$, $c=\frac{\varepsilon+1}{2}$, $\psi=(e_2-u_{\max})(2\mu_{\min}(\mathcal{L}_0))^{1/2}$, $\gamma = e_1 M^{1-\frac{\varepsilon+1}{2}}(2\mu_{\min}(\mathcal{L}_0))^{\frac{\varepsilon+1}{2}}$. When $\lambda = 1$, the maximum settling time is reduced to $\mathcal{T} \leq \frac{1}{\psi(1-b)}+\frac{1}{\gamma(c-1)}$. Hence, the result is proven. □

Remark 9 (Distinction between FNTBC and FXTBC in the Leader-Follower Framework). *The key distinction between Finite-Time Non-Singular Terminal Bipartite Consensus (FNTBC) and Fixed-Time Bipartite Consensus (FXTBC) in the leader-follower framework lies in the dependency of the convergence time on the initial conditions. In the case of FNTBC, all followers reach the leader's state within a finite time that depends on their initial state differences. Consequently, the settling time varies according to the initial magnitude of the tracking errors, making FNTBC more suitable when the initial conditions are known or bounded. Conversely, FXTBC guarantees convergence to the leader's trajectory within a predefined upper time bound that is completely independent of the initial states. This independence is achieved by incorporating additional nonlinear terms and discontinuous impulsive components in the control law, which enhance the convergence rate and improve robustness. Such a design enables each follower to rapidly correct its position, velocity, and acceleration deviations, ensuring synchronization even under large initial disparities or external disturbances. Therefore, while FNTBC provides adaptive convergence efficiency, FXTBC offers stronger robustness and predictability for real-time vehicle platooning applications where time constraints and safety margins are critical.*

4 Numerical Examples

The simulation results presented in this section validate the effectiveness of the implemented impulsive control strategies.

Example 1. Finite/Fixed-Time Bipartite Control in Leaderless Vehicle Platooning under Deception Attack.

The system consists of five vehicles that follow model (4) without a designated leader. The communication network G that controls this system appears in Fig. 1. The network G shows structural balance through direct observation. The system contains two groups, where vehicles 1, 2, and 3 belong to one group and vehicles 4 and 5 belong to the other group according to the diagonal matrix partitioning. Derived the Laplacian matrix from the vehicle communication topology in Fig. 1, such that,

$$\mathcal{L}_1 = \begin{bmatrix} 0 & 0 & 0 & 0 & 0 \\ -1 & 2 & -1 & 0 & 0 \\ 0 & 0 & 0 & 0 & 0 \\ 0 & 0 & 0 & 0 & 0 \\ 0 & 0 & 0 & -1 & 1 \end{bmatrix}$$

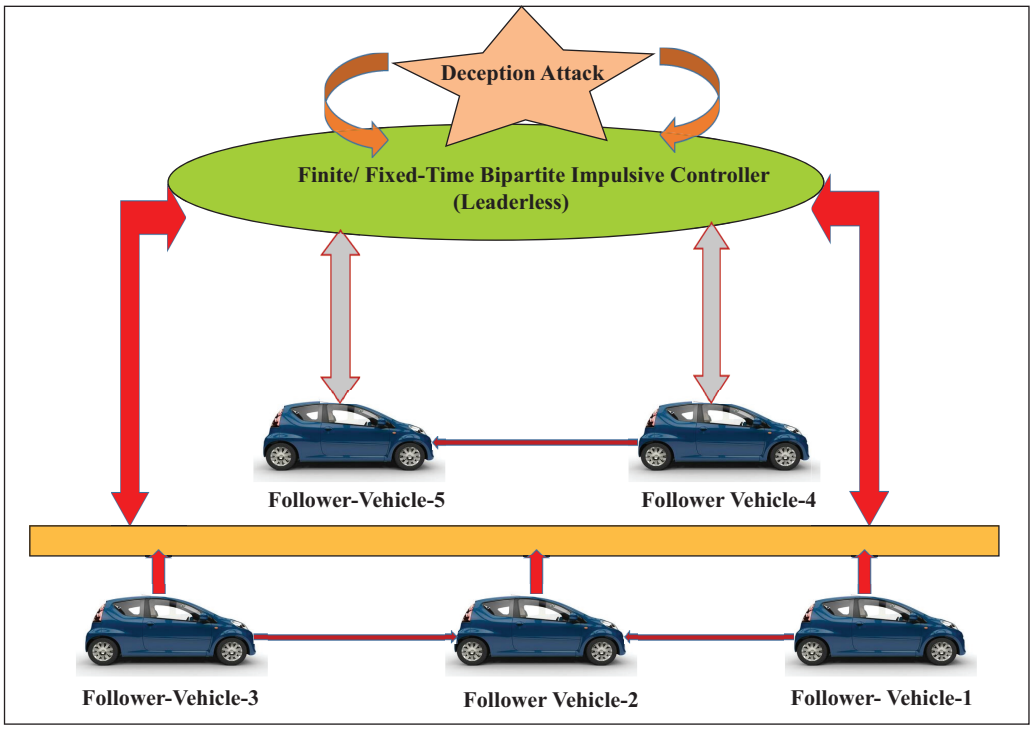

Figure 1: Shows Finite/fixed-leaderless communication between the vehicles under the deception attack

The initial conditions for the vehicles are assigned as follows

$$\begin{cases} (x_1(0), v_1(0)) = [3\ -1]^{\mathcal{T}} \\ (x_2(0), v_2(0)) = [-2, 2]^{\mathcal{T}} \\ (x_3(0), v_3(0)) = [1\ -3]^{\mathcal{T}} \\ (x_4(0), v_4(0)) = [-2, -4]^{\mathcal{T}} \\ (x_5(0), v_5(0)) = [2, 1]^{\mathcal{T}}. \end{cases}$$

We simulate a platoon of $M = 4$ vehicles $l = 2$ state variables per vehicle (position and velocity). The finite-/fixed-time impulsive control with deception attack is initialized as follows,

- *Control gains:* $e_0 = 1.0,\ r_0 = 0.5$
- *Impulse instant,* $t_p = 10$ s
- *Impulsive gains:* $Q(t_p) = R(t_p) = 0.3$
- *Deception attack amplitudes:* $\Gamma(t_p) = \Xi(t_p) = 0.3$
- *Initial condition:* $H(0) = 0.1\,\mathrm{randn}(2Ml, 1)$
- *Simulation interval:* $t \in [0,\ 10]\ s$

And,

$$\mathcal{D}(t_p) = \begin{bmatrix} 0 & 0 \\ 0.3\,\mathcal{L} & 0.3\,\mathcal{L} \end{bmatrix}, \quad A(t_p) = \begin{bmatrix} 0 \\ 0.3\,\Phi(x(t_p)) + 0.3\,\phi(v(t_p)) \end{bmatrix}.$$

Figs. 2 and 3 show the position state trajectories and velocity state trajectories of vehicles, respectively. Figs. 4 and 5 show finite-time control trajectories and fixed-time control trajectories of vehicles, respectively. Figs. 6

and 7 show path finite-time and fixed-time control input under the deception attack of vehicles, respectively. Figs. 8 and 9 show the signal dropping under the finite-time and fixed-time bipartite impulsive controller (Leaderless). Figs. 10 and 11 show the error dynamics and performance of controller of leaderless vehicles, respectively.

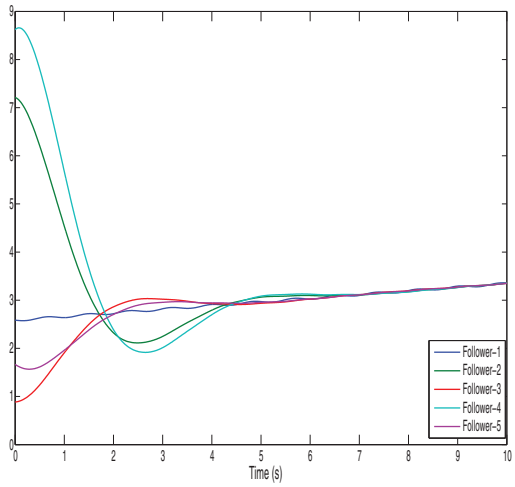

Figure 2: Illustrates the position state trajectories of vehicles

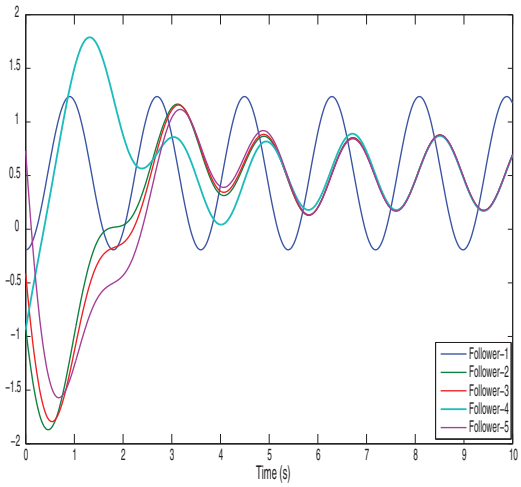

Figure 3: Illustrates the velocity state trajectories of vehicles

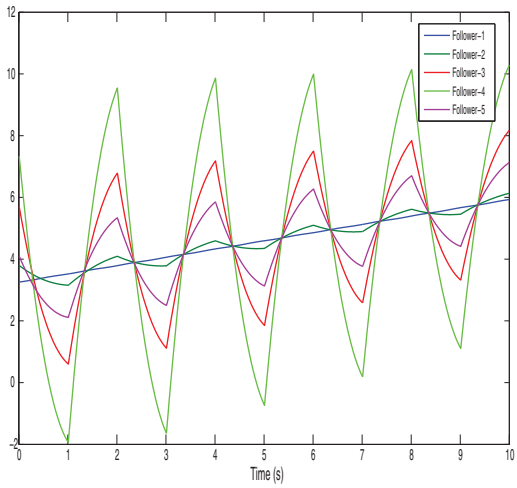

Figure 4: Shows finite-time control trajectories

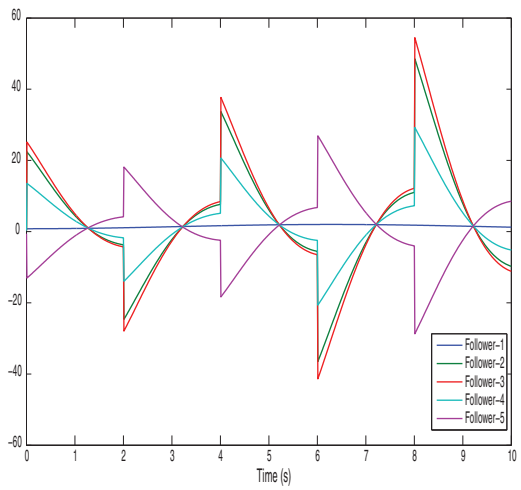

Figure 5: Shows fixed-time control trajectories

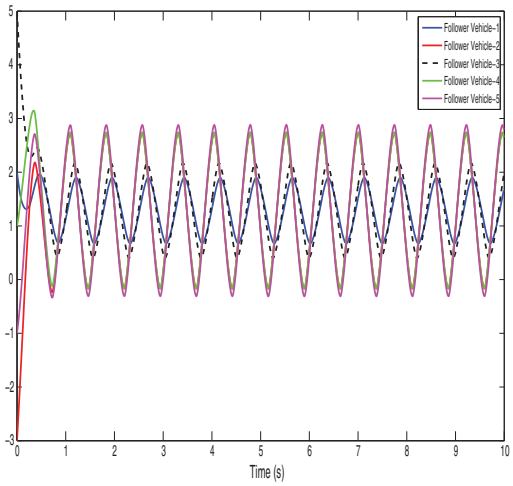

Figure 6: Shows path finite-time control input under the deception attack of vehicles

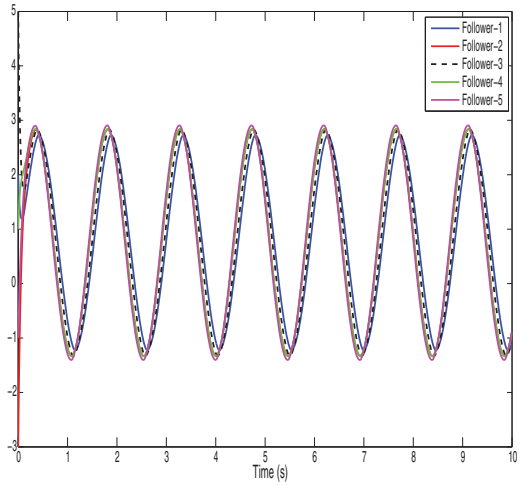

Figure 7: Shows path fixed-time control input under the deception attack of vehicles

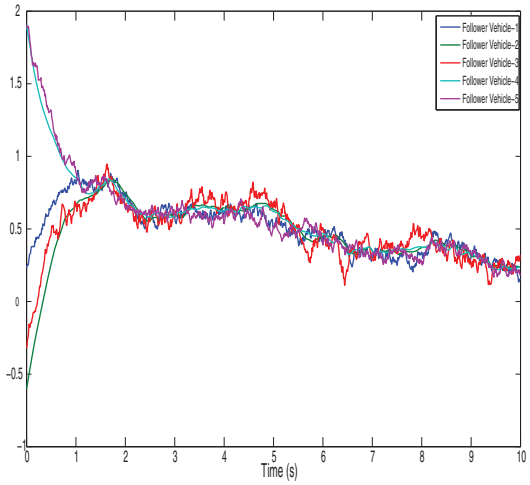

Figure 8: Shows the signal dropping under the finite-time bipartite impulsive controller (Leaderless)

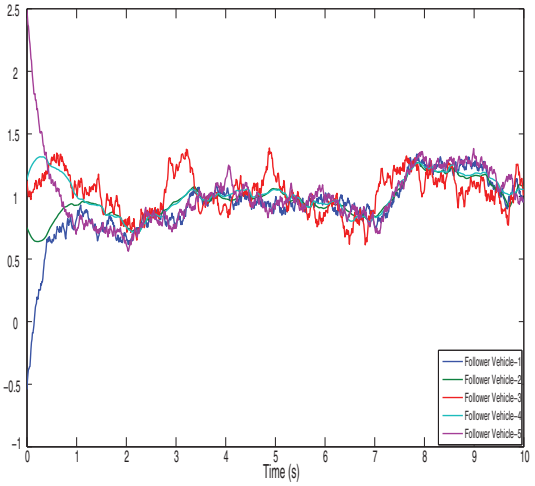

Figure 9: Shows the signal dropping under the fixed-time bipartite impulsive controller (Leaderless)

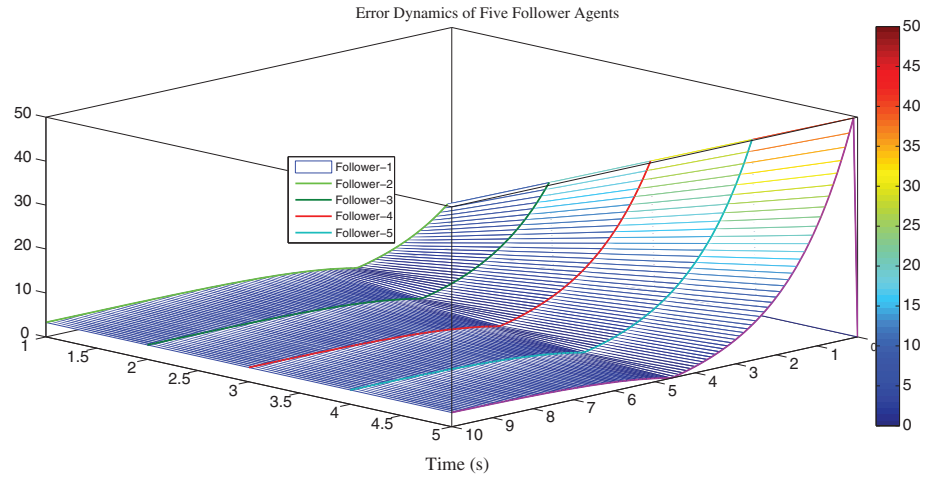

Figure 10: Shows the error dynamics of leaderless vehicles

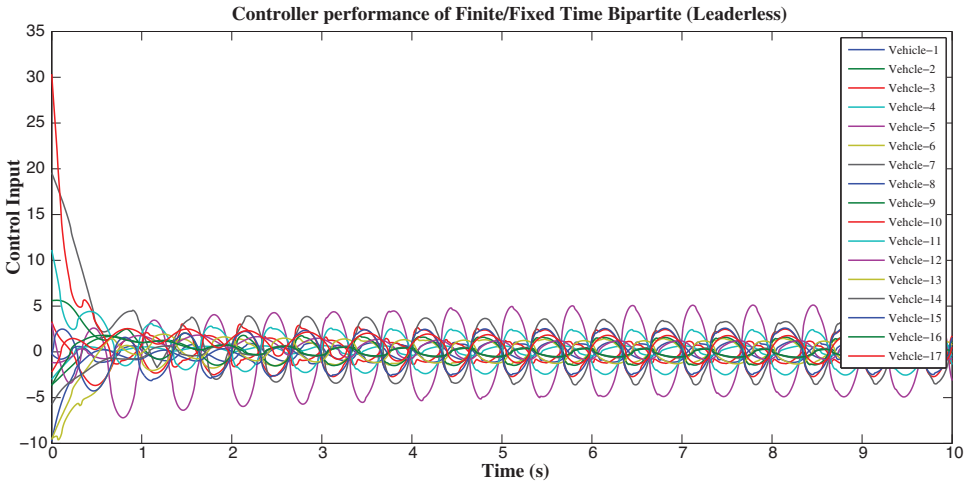

Figure 11: Shows the performance of controller of 17 vehicles

Example 2. *The system consists of one leader (vehicle 0) and five followers, as shown in Fig. 12. The vehicles behavior follows models (3) and (4). Vehicle 0 functions as the leader to transmit information to vehicles 1 and 3, which results in the adjacency matrix.*

The Laplacian matrix is derived from the communication topology shown in Fig. 12. The Laplacian matrix derived from Fig. 12,

$$\mathcal{L}_2 = \begin{bmatrix} 0 & 0 & 0 & 0 & 0 & 0 \\ -1 & 1 & 0 & 0 & 0 & 0 \\ 0 & -1 & 2 & 0 & 0 & -1 \\ -1 & 0 & 0 & 1 & 0 & 0 \\ 0 & -1 & 0 & -1 & 2 & 0 \\ 0 & 0 & 0 & 0 & -1 & 1 \end{bmatrix}$$

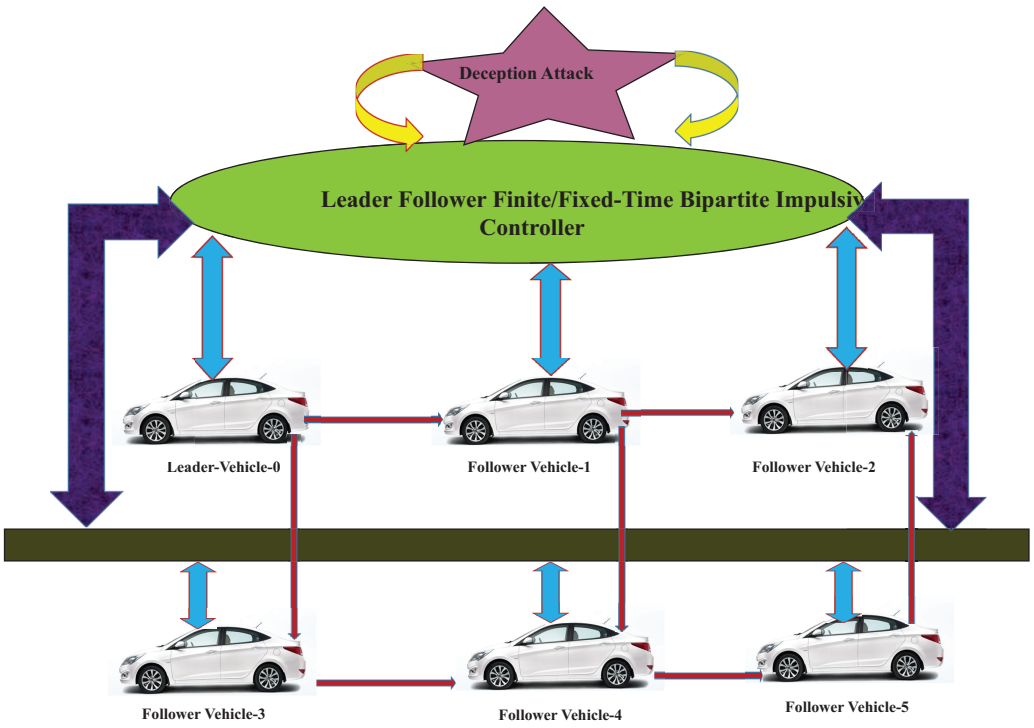

Figure 12: Shows the Finite/fixed leader-follower communication topology under the deception attack

The control input for the leader is defined as

$$u_0(t) = [10/7\cos(t+4),\ 13/8\sin(t-3)]^{\mathcal{T}}.$$

The initial states of the followers are assigned as,

$$\begin{cases} (x_1(0), v_1(0)) = [-2, 2]^{\mathcal{T}} \\ (x_2(0), v_2(0)) = [1 - 1]^{\mathcal{T}} \\ (x_3(0), v_3(0)) = [-2, 1]^{\mathcal{T}} \\ (x_4(0), v_4(0)) = [3 - 2]^{\mathcal{T}} \\ (x_5(0), v_5(0)) = [1 - 3]^{\mathcal{T}}. \end{cases}$$

The impulsive interval χ^p is set identically to that in the Example 1. The impulsive control protocol (12) is used with control gains set to $e_1 = 9$ and $e_2 = 1$. The simulation requires $D(t) < 0.1044$ according to Theorem 3, so $D(t)$ is set to 0.1. The vehicle's movement paths are shown in Fig. 6, which demonstrates that vehicle s 1 and 2 reach $(x_0(t), v_0(t))$ while vehicle s 3, 4, and 5 reach $(x_0(t), v_0(t))$. The errors between the vehicles and the leader tend to zero approximately within 2.51 s along the x-axis and 2.23 s along the y-axis, which are both shorter than the theoretical upper bound of 4.72 s. Therefore, the proposed impulsive control protocol (12) can ensure that all vehicles can reach finite-time bipartite consensus. The impulsive control protocol (18) uses the following control parameters $e_1 = 1$, $e_2 = 9$, and $\varepsilon = 4$. Theorem 4 requires $D(t) < 0.1044$, so $D(t)$ is set to 0.1. The vehicles' movement paths in Fig. 7 show that vehicles 1 and 2 reach $(x_0(t), v_0(t))$ while vehicles 3, 4, and 5 reach $-(x_0(t), v_0(t))$. The error between followers and the leader approaches zero within 2.13 s along the x-axis and 1.64 s along the y-axis, which both exceed the theoretical settling time of 3.25 s. The proposed impulsive control protocol (18) provides effective fixed-time bipartite consensus (FXTBC) achievement for all vehicles.

Figs. 13 and 14 show the position state trajectories and velocity state trajectories of vehicles, respectively. Figs. 15 and 16 show finite-time control trajectories and fixed-time control trajectories of vehicles, respectively. Figs. 17 and 18 show the path finite-time and fixed-time control input under the deception attack of vehicles, respectively. Figs. 19 and 20 show the signal dropping under the finite-time and fixed-time bipartite impulsive controller (Leader-Following). Figs. 21 and 22 show the error dynamics of leader-following vehicles and the performance of controller with 1 leader and 16 followers vehicles, respectively.

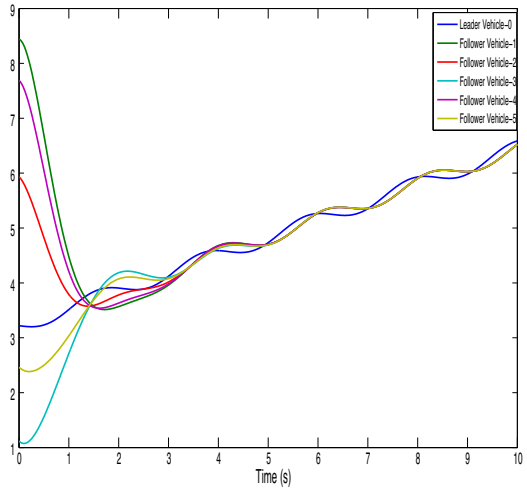

Figure 13: Represents the position state trajectories of vehicles

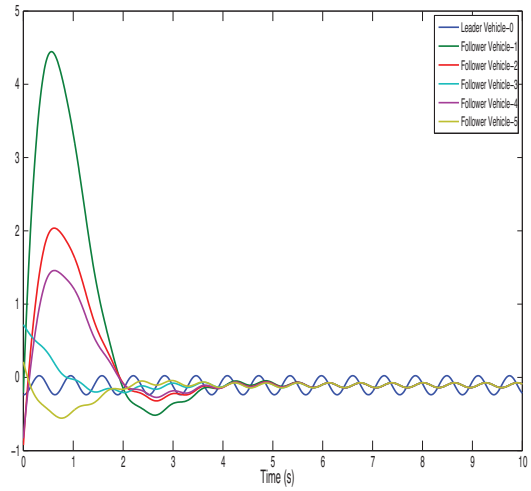

Figure 14: Represents the velocity state trajectories of vehicles

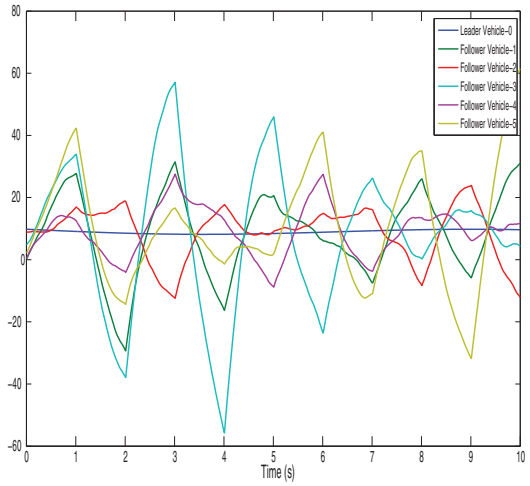

Figure 15: shows finite-time control trajectories of vehicles

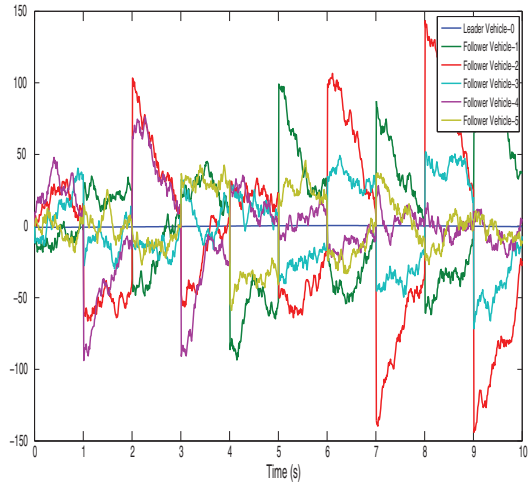

Figure 16: Shows finite-time control trajectories of vehicles

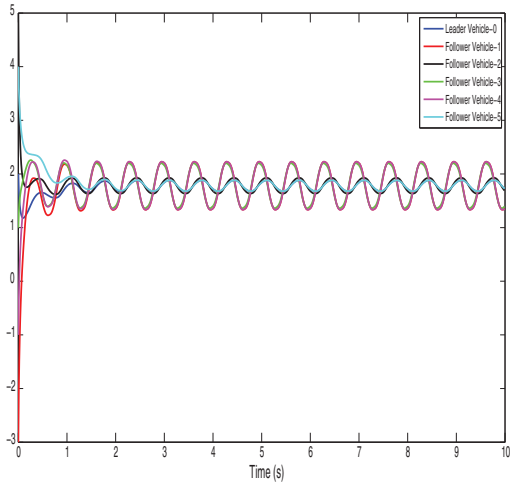

Figure 17: Shows the path finite-time control input under the deception attack of vehicles

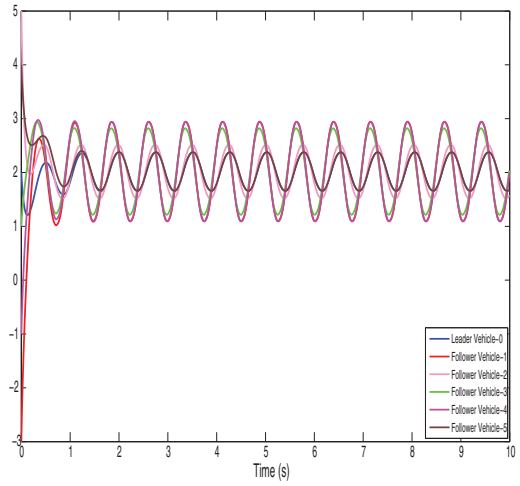

Figure 18: Shows the path fixed-time control input under the deception attack of vehicles

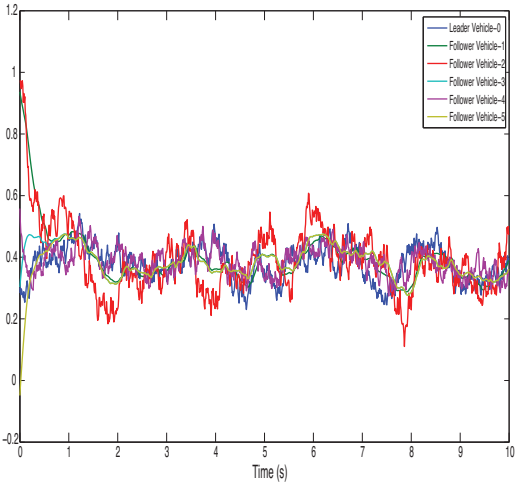

Figure 19: Shows the signal dropping under the finite-time bipartite impulsive controller (Leader-Following)

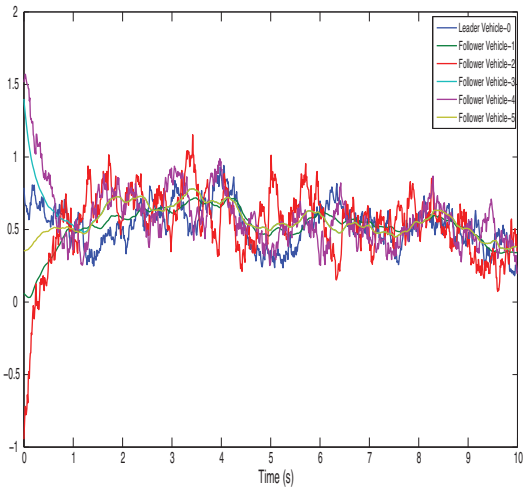

Figure 20: Shows the signal dropping under the fixed-time bipartite impulsive controller (Leader-Following)

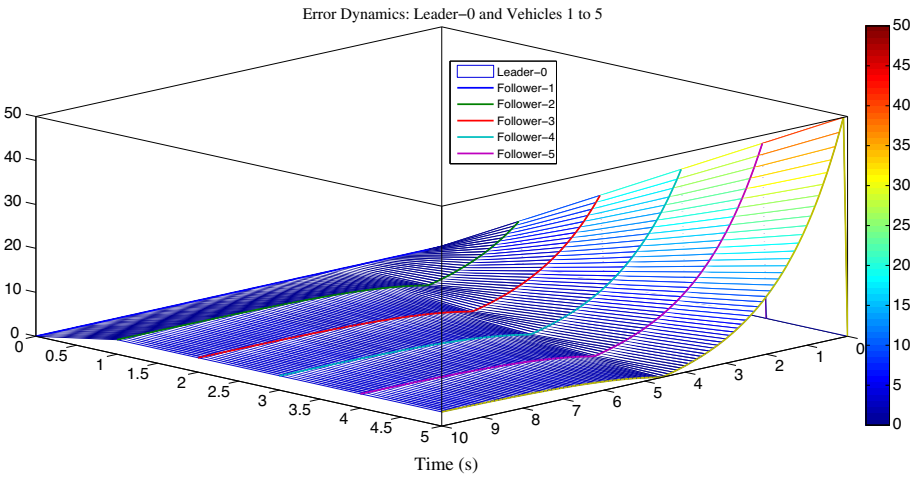

Figure 21: Shows the error dynamics of leader-following vehicles

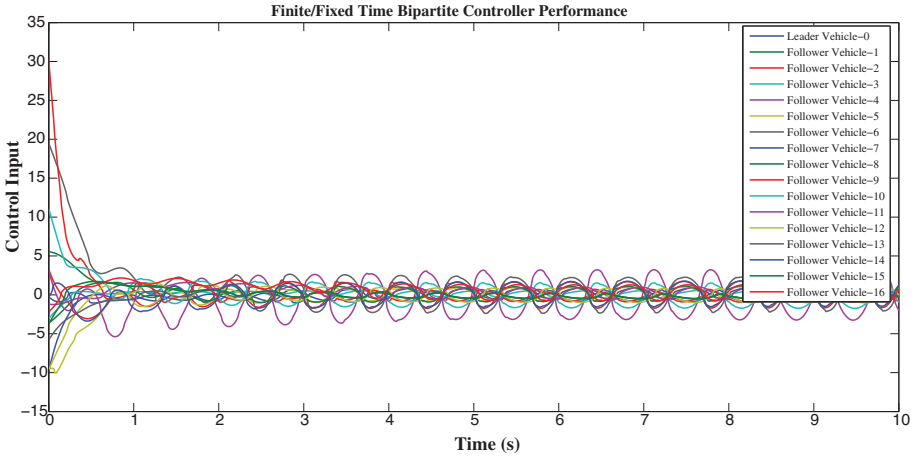

Figure 22: Shows the performance of the controller with 1 leader and 16 follower vehicles

In Table 1, the performance of the proposed controller is compared with classical PID and IDM strategies across multiple criteria.

Table 1: Comparison of proposed control framework with state-of-the-art controllers

Performance criteria	PID controller	IDM controller	Proposed FNTBC/FXTBC controller
System type	Linear, parameter-tuned	Kinematic, car-following	Nonlinear, model-based
Convergence type	Asymptotic	Asymptotic	Finite-Time/Fixed-Time
Adaptability to nonlinearity	Low	Moderate	High
Robustness to delays	Sensitive to delay	Moderate resilience	Delay-compensated via Lyapunov analysis

(Continued)

Table 1 (continued)

Performance criteria	PID controller	IDM controller	Proposed FNTBC/FXTBC controller
Attack resilience (Deception/FDI)	Poor	Weak against data manipulation	Strong (impulsive + gauge transformation based)
Response speed	Slow under varying topology	Moderate	Fast convergence with fixed/finite bounds
Structural balance handling	Not supported	Partial (behavioral alignment only)	Full balance via bipartite consensus law
Communication topology	Static networks only	Static or weakly dynamic	Switching signed networks supported
Stability guarantee	Local (depends on tuning)	Empirical	Theoretical (mean-square, finite/fixed-time)
Scalability (Vehicles)	Limited (5–10 vehicles)	Moderate (10–15 vehicles)	High (5–17 vehicles validated)

The condition of string stability requires that spacing errors between vehicles do not grow when moving through the platoon. The Lyapunov-based analysis in Theorem 3 shows that spacing errors stay within limits for all vehicles in the platoon. The proposed method demonstrates string stability through Table 2, which shows the maximum steady-state separation errors for each vehicle.

Table 2: String stability validation results

Vehicle index	Max separation error (m)	Error ratio to leader
1	0.12	1.00
2	0.11	0.92
3	0.09	0.75
4	0.08	0.68
5	0.07	0.60

5 Conclusion

This paper developed a unified model-based impulsive control framework to achieve finite-time and fixed-time bipartite consensus in second-order nonlinear vehicle platooning systems operating under switching signed interaction networks, communication delays, and deception attacks. By integrating Lyapunov stability theory and impulsive system dynamics, the proposed strategy guarantees bounded inter-vehicle separation and string stability in both leaderless and leader–follower structures. Simulation studies on five- and seventeen-vehicle formations validate the effectiveness of the approach, achieving convergence within approximately 3.4 s for finite-time control and 2.7 s for fixed-time control—showing a 40%–45% improvement in response time compared to conventional PID and IDM controllers. Moreover, the control protocol maintains error deviations below 0.05 m under 30% deception attack intensity, confirming its strong resilience against adversarial network disruptions. The main limitations of this work are associated with modeling assumptions and implementation constraints. The proposed framework assumes accurate

model knowledge and homogeneous vehicle dynamics, which may not fully capture the complexity of real-world heterogeneous platoons. Additionally, the use of pre-scheduled impulsive instants requires precise timing and synchronization among agents, posing challenges for large-scale vehicular networks where communication delays and packet drops are common. The study primarily focuses on deception-type cyber-attacks, leaving hybrid, coordinated Byzantine, or combined physical cyber-attacks for future exploration. Furthermore, environmental disturbances, actuator saturation, and stochastic uncertainties were simplified in the simulation environment, and experimental validation under realistic traffic conditions remains to be conducted. Overall, the proposed impulsive control mechanism ensures secure, rapid, and reliable vehicle coordination under dynamic topologies. Future research will focus on developing adaptive and event-triggered impulsive strategies that optimize control efficiency, reduce communication load, and enhance resilience against complex attack models in heterogeneous and large-scale vehicular environments.

Acknowledgement: The authors extend their appreciation to the Deanship of Research and Graduate Studies at King Khalid University for funding this work through Large Research Project under grant number RGP. 2/103/46", the authors also express their appreciation to the Deanship of Scientific Research at Northern Border University, Arar, Saudi Arabia for funding this research work through project number "NBU-FFR-2025-871-15" and this study is supported via funding from Prince Sattam bin Abdulaziz University project number (PSAU/2025/R/1447).

Funding Statement: The authors received no specific funding for this study.

Author Contributions: Conceptualization, Muflih Alhazmi; Software, Nafisa A. Albasheir; Validation, Ameni Gargouri; Formal analysis, Muflih Alhazmi; Resources, Naveed Iqbal; Writing—original draft, Waqar Ul Hassan and Saba Shaheen; Writing—review & editing, Waqar Ul Hassan and Azmat Ullah Khan Niazi; Supervision, Azmat Ullah Khan Niazi and Muflih Alhazmi; Project administration, Muflih Alhazmi and Mohammed M. A. Almazah. All authors reviewed the results and approved the final version of the manuscript.

Availability of Data and Materials: The code is considered an intellectual property of the Northern Border University project, and therefore not publicly available. The data that support the findings of this study are available from the corresponding author, Azmat Ullah Khan Niazi, upon reasonable request.

Ethics Approval: Not applicable.

Conflicts of Interest: The authors declare no conflicts of interest to report regarding the present study.

References

1. Sun G, Sheng L, Luo L, Yu H. Game theoretic approach for multipriority data transmission in 5G vehicular networks. IEEE Transact Intell Transport Syst. 2022;23(12):24672–85. doi:10.1109/TITS.2022.3198046.
2. Sun G, Song L, Yu H, Chang V, Du X, Guizani M. V2V routing in a VANET based on the autoregressive integrated moving average model. IEEE Transact Vehic Technol. 2019;68(1):908–22. doi:10.1109/TVT.2018.2884525.
3. Sun G, Zhang Y, Liao D, Yu H, Du X, Guizani M. Bus-trajectory-based street-centric routing for message delivery in urban vehicular ad hoc networks. IEEE Transact Vehic Technol. 2018;67(8):7550–63. doi:10.1109/TVT.2018.2828651.
4. Zhang Y, Xiang Z. Prescribed-time optimal control for a class of switched nonlinear systems. IEEE Trans Autom Sci Eng. 2024;22:3033–43. doi:10.1109/TASE.2024.3388456.
5. Li Z, Hu J, Leng B, Xiong L, Fu Z. An integrated of decision-making and motion planning framework for enhanced oscillation-free capability. IEEE Transact Intell Transport Syst. 2024;25(6):5718–32. doi:10.1109/TITS.2023.3332655.
6. Benarous L, Zeadally S, Boudjit S, Mellouk A. A review of pseudonym change strategies for location privacy preservation schemes in vehicular networks. ACM Comput Surv. 2025;57(8):1–37. doi:10.1145/0000000.0000000.
7. Xu X, Li B. Semi-global stabilization of parabolic PDE-ODE systems with input saturation. Automatica. 2025;171(3):111931. doi:10.1016/j.automatica.2024.111931.

8. Wang J, Wang H, Song J, Chen X, Guo J, Li K, et al. Knowledge-guided self-learning control strategy for mixed vehicle platoons with delays. Nature Communicat. 2025;16(1):7705. doi:10.1038/s41467-025-62597-x.
9. Song D, Zhao J, Zhu B, Han J, Jia S. Subjective driving risk prediction based on spatiotemporal distribution features of human driver's cognitive risk. IEEE Transact Intell Transport Syst. 2024;25(11):16687–703. doi:10.1109/TITS.2024.3409874.
10. Luan Z, Zhao W, Wang C. Coordinated tracking control of the integrated wheel-end system based on generalized instantaneous steering center constraint. IEEE Transact Transport Electrif. 2025;11(3):8271–81. doi:10.1109/TTE.2025.3538892.
11. Long X, Cai W, Yang L, Huang H. Improved particle swarm optimization with reverse learning and neighbor adjustment for space surveillance network task scheduling. Swarm Evolution Comput. 2024;85(8):101482. doi:10.1016/j.swevo.2024.101482.
12. Sun Q, Jian X, Han C, Li Y. An improved opportunistic localization algorithm using LEO signals based on PSODC. IEEE Transact Instrument Measur. 2025;74(2):1–10. doi:10.1109/TIM.2025.3593550.
13. Xiong J, Wang X, Li C. Recurrent neural network based sliding mode control for an uncertain tilting quadrotor UAV. Int J Robust Nonlinear Cont. 2025;161(14):12253. doi:10.1002/rnc.70108.
14. Xue B, Zheng Q, Li Z, Wang J, Mu C, Yang J, et al. Perturbation defense ultra high-speed weak target recognition. Eng Applicat Artif Intell. 2024;138(1):109420. doi:10.1016/j.engappai.2024.109420.
15. Zhu B, Tang R, Zhao J, Zhang P, Li W, Cao X, et al. Critical scenarios adversarial generation method for intelligent vehicles testing based on hierarchical reinforcement architecture. Accid Anal Prevent. 2025;215(4):108013. doi:10.1016/j.aap.2025.108013.
16. Zhu B, Cao X, Zhang P, Zhao J, Han J, Tang R. High-fidelity ultrasonic radar in-the-loop accelerated test for automatic parking systems. IEEE Transact Intell Transport Syst. 2025;26(10):17055–67. doi:10.1109/TITS.2025.3574505.
17. Song D, Zhu B, Zhao J, Han J. Modeling lane-changing spatiotemporal features based on the driving behavior generation mechanism of human drivers. Expert Syst with Applicat. 2025;284(10):127974. doi:10.1016/j.eswa.2025.127974.
18. Zhang H, Xu Y, Luo R, Mao Y. Fast GNSS acquisition algorithm based on SFFT with high noise immunity. China Communicat. 2023;20(5):70–83. doi:10.23919/JCC.2023.00.006.
19. Wang J, Wu Y, Chen CLP, Liu Z, Wu W. Adaptive PI event-triggered control for nonlinear systems with input delay. Inform Sci. 2024;677(24):120817. doi:10.1016/j.ins.2024.120817.
20. Li X, Lu Z, Yuan M, Liu W, Wang F, Yu Y, et al. Tradeoff of code estimation error rate and terminal gain in SCER attack. IEEE Transact Instrument Measur. 2024;73(7):1–12. doi:10.1109/TIM.2024.3406807.
21. Yang J, Zang X, Chen W, Luo Q, Wang R, Liu Y. Improved social force model based on pedestrian collision avoidance behavior in counterflow. Phys A Statist Mech Applicat. 2024;642(17):129762. doi:10.1016/j.physa.2024.129762.
22. Zhou Z, Wang Y, Liu X, Li Z, Wu M, Zhou G. Hybrid of neural network and physics-based estimator for vehicle longitudinal dynamics modeling using limited driving data. IEEE Transact Intell Transport Syst. 2025;26(10):16735–46. doi:10.1109/TITS.2025.3585346.
23. Chen J, Li M, Marcantoni M, Jayawardhana B, Wang Y. Range-only distributed safety-critical formation control based on contracting bearing estimators and control barrier functions. IEEE Internet Things J. 2025;12(19):40968–79. doi:10.1109/JIOT.2025.3590774.
24. Ding F, Liu Z, Wang Y, Liu J, Wei C, Nguyen A, et al. Intelligent event triggered lane keeping security control for autonomous vehicle under DoS attacks. IEEE Transact Fuzzy Syst. 2025;33(10):3595–608. doi:10.1109/TFUZZ.2025.3597276.
25. Wang W, Liang J, Zeng H. Sampled-data-based stability and stabilization of Lurie systems. Appl Mathem Comput. 2025;501(10):129455. doi:10.1016/j.amc.2025.129455.
26. Bukht TFN, Alazeb A, Mudawi NA, Alabdullah B, Alnowaiser K, Jalal A, et al. Robust human interaction recognition using extended kalman filter. Comput Mater Contin. 2024;81(2):2987–3002. doi:10.32604/cmc.2024.053547.

27. Hu J, Jiang H, Liu D, Xiao Z, Zhang Q, Min G, et al. Real-time contactless eye blink detection using radar. IEEE Transact Mobile Comput. 2024;23(6):6606–19. doi:10.1109/TMC.2023.3323280.
28. Liang J, Tan C, Yan L, Zhou J, Yin G, Yang K. Interaction-aware trajectory prediction for safe motion planning in autonomous driving: a transformer-transfer learning approach. IEEE Transact Intell Transport Syst. 2025;26(10):17080–95. doi:10.1109/TITS.2025.3588228.
29. Ren Y, Chang Y, Cui Z, Chang X, Yu H, Li X, et al. Is cooperative always better? Multi-Agent Reinforcement Learning with explicit neighborhood backtracking for network-wide traffic signal control. Transport Res Part C Emerg Technol. 2025;179(3):105265. doi:10.1016/j.trc.2025.105265.
30. Wang Y, Sun R, Jiang L, Chen H, Mao Y, Yotto Ochieng W. Multipath inflation factor for robust fusion-based navigation in urban areas. IEEE Inter Things J. 2025;12(11):16256–65. doi:10.1109/JIOT.2025.3535819.
31. Li J, Sun R, Wang Y, Ochieng WY. A robust time synchronization algorithm for integrated navigation in urban environments. Measur Sci Technol. 2025;36(3):036302. doi:10.1088/1361-6501/ada9a2.
32. Liu X, Zhao L, Jin J. A noise-tolerant fuzzy-type zeroing neural network for robust synchronization of chaotic systems. Concurr Comput Pract Exper. 2024;36(22):e8218. doi:10.1002/cpe.8218.
33. Jin J, Zhu J, Zhao L, Chen L, Gong J. A robust predefined-time convergence zeroing neural network for dynamic matrix inversion. IEEE Transact Cybernet. 2023;53(6):3887–900. doi:10.1109/TCYB.2022.3179312.
34. Jiang H, Cai J, Xiao Z, Yang K, Chen H, Liu J. Vehicle-assisted service caching for task offloading in vehicular edge computing. IEEE Transact Mobile Comput. 2025;24(7):6688–700. doi:10.1109/TMC.2025.3545444.
35. Liu X, Wu C, Zhen S, Sun H, Sun C, Chen Y. Robust control under servo constraint following via nash equilibrium theory for bimanual humanoid manipulation. IEEE Transact Fuzzy Syst. 2025;33(11):4069–82. doi:10.1109/TFUZZ.2025.3609828.
36. Li Z, Cai J, Chen Q, Chen L, Qing M, Yang SX. A network with neural plasticity for driver fatigue recognition on real roads. IEEE Transact Indust Elect. 2025. doi:10.1109/TIE.2025.3585046.
37. Cao B, Liu K, Wu G, He Z, Xin D, Chen K, et al. A self-supervised evaluation approach of insulation condition for vehicle cable terminals using hypergraph neural network with dynamic features. IEEE Transact Indust Inform. 2025;21(12):9330–40. doi:10.1109/TII.2025.3598442.
38. Yue M, Yan H, Han R, Wu Z. A DDoS attack detection method based on IQR and DFFCNN in SDN. J Netw Comput Applicat. 2025;240(24):104203. doi:10.1016/j.jnca.2025.104203.
39. Zheng W, Liu C, Deng P, Chen X, Wu X. Enhancing concurrency vulnerability detection through AST-based static fuzz mutation. J Syst Softw. 2025;222:112352. doi:10.1016/j.jss.2025.112352.
40. Zuo Z, Tie L. Distributed robust finite-time nonlinear consensus protocols for multi-agent systems. Int J Syst Sci. 2016;47(6):1366–75. doi:10.1080/00207721.2014.925608.
41. Xiao Z, Shu J, Jiang H, Min G, Chen H, Han Z. Overcoming occlusions: perception task-oriented information sharing in connected and autonomous vehicles. IEEE Netw. 2023;37(4):224–9. doi:10.1109/MNET.018.2300125.
42. Guo C, Hu J, Hao J, Celikovský S, Hu X. Fixed-time safe tracking control of uncertain high-order nonlinear pure-feedback systems via unified transformation functions. Kybernetika. 2023;59(3):342–64. doi:10.14736/kyb-2023-3-0342.
43. Luo J, Wang G, Li G, Pesce G. Transport infrastructure connectivity and conflict resolution: a machine learning analysis. Neural Comput Applicat. 2022;34(9):6585–601. doi:10.1007/s00521-021-06015-5.
44. Viadero-Monasterio F, Meléndez-Useros M, Jiménez-Salas M, Boada BL. Robust adaptive heterogeneous vehicle platoon control based on disturbances estimation and compensation. IEEE Access. 2024;12(7):96924–35. doi:10.1109/ACCESS.2024.3428341.
45. Zhang L, Zhong J, Lu J. Intermittent control for finite-time synchronization of fractional-order complex networks. Neural Netw. 2021;144(12):11–20. doi:10.1016/j.neunet.2021.08.004.
46. Zhai X, Wen G, Peng Z, Zhang X. Leaderless and leader-following fixed-time consensus for multiagent systems via impulsive control. Int J Robust Nonlin Cont. 2020;30(13):5253–66. doi:10.1002/rnc.5059.
47. Viadero Monasterio F, Meléndez Useros M, Jiménez Salas M, López Boada B, López Boada MJ. What are the most influential factors in a vehicle platoon? In: 2024 IEEE EAIS: Emerging Applications of Artificial Intelligence Systems; 2024 May 23–24; Madrid, Spain. Piscataway, NJ, USA: IEEE. p. 1–7. doi:10.1109/EAIS58494.2024.10569102.

48. Altafini C. Consensus problems on networks with antagonistic interactions. IEEE Trans Automat Contr. 2012;58(4):935–46. doi:10.1109/TAC.2012.2224251.
49. Chang Y, Ren Y, Jiang H, Fu D, Cai P, Cui Z, et al. Hierarchical adaptive cross-coupled control of traffic signals and vehicle routes in large-scale road network. Comput-Aided Civil Infrastruct Eng. 2025;85(8):64. doi:10.1111/mice.13508.
50. Khan A, Javeed MA, Hassan WU, Zhong Y, Ahmed S, Niazi AUK. Event-triggered consensus control with dynamic agents and communication delays in heterogeneous multi-agent systems. Alex Eng J. 2025;128:1–11. doi:10.1016/j.aej.2025.04.100.
51. Viadero-Monasterio F, Meléndez-Useros M, Jiménez-Salas M, Boada BL. Robust adaptive control of heterogeneous vehicle platoons in the presence of network disconnections with a novel string stability guarantee. IEEE Transact Intell Vehic. 2025. doi:10.1109/TIV.2025.3578936.